

Tensor-Efficient High-Dimensional Q-learning

Junyi Wu

Department of Industrial & System Engineering
University of Washington
junyiwu@uw.edu

Dan Li

Department of Industrial & System Engineering
University of Washington
dli27@uw.edu

Abstract

High-dimensional reinforcement learning (RL) faces challenges with complex calculations and low sample efficiency in large state-action spaces. Q-learning algorithms struggle particularly with the curse of dimensionality, where the number of state-action pairs grows exponentially with problem size. While neural network-based approaches like Deep Q-Networks have shown success, they do not explicitly exploit problem structure. Many high-dimensional control tasks exhibit low-rank structure in their value functions, and tensor-based methods using low-rank decomposition offer parameter-efficient representations. However, existing tensor-based Q-learning methods focus on representation fidelity without leveraging this structure for exploration. We propose Tensor-Efficient Q-Learning (TEQL), which represents the Q-function as a low-rank CP tensor over discretized state-action spaces and exploits the tensor structure for uncertainty-aware exploration. TEQL incorporates Error-Uncertainty Guided Exploration (EUGE), which combines tensor approximation error with visit counts to guide action selection, along with frequency-aware regularization to stabilize updates. Under matched parameter budgets, experiments on classic control tasks demonstrate that TEQL outperforms both matrix-based low-rank methods and deep RL baselines in sample efficiency, making it suitable for resource-constrained applications where sampling costs are high.

Keywords: reinforcement learning, tensor decomposition, Q-learning, sample efficiency, high-dimensional

1 Introduction

Value function estimation is the basic computational challenge in reinforcement learning, where agents must evaluate the expected cumulative rewards associated with states or state-action pairs to guide optimal decision-making (Sutton and Barto, 2018; Bellman, 1957; Bertsekas and Tsitsiklis, 1996). The value function provides the fundamental link between observed rewards and long-term planning, with theoretical foundations rooted in dynamic programming and Markov Decision Processes (Puterman, 1994; Bertsekas and Tsitsiklis, 1996; Szepesvari, 2010). Recent work has further revealed structural properties of value functions that can be exploited for efficient learning (Dadashi et al., 2019; Yang et al., 2020).

This challenge becomes particularly acute in high-dimensional state-action spaces with inherent discrete structure, which arise naturally in operations research and industrial systems. In these domains, state and action spaces factorize into multiple discrete components, and the total number of configurations grows exponentially in the number of dimensions, creating severe computational and statistical burdens.

Two representative settings illustrate this structure. In clinical treatment optimization, the state of a patient is described by multiple discrete clinical indicators such as severity levels, organ function grades, and recovery stages, and the treatment decision is a combination of discrete choices among drugs, dosages, and interventions (Komorowski et al., 2018; Liu et al., 2019). The state-action space grows combinatorially with the number of clinical dimensions, yet drug interactions are predominantly pairwise, with higher-order interactions among three or more treatments being rare in practice, which implies that the value function admits low-rank tensor structure. Each treatment trial involves a real patient, making data collection expensive and sample-efficient learning essential. In multi-echelon inventory management, the state is the vector of discrete inventory levels across all stock-

ing locations, and the action is the joint replenishment decision specifying an integer order quantity at each location. The state-action space grows exponentially with the number of locations, yet the optimal policy often admits low-rank structure because demands are driven by a small number of shared factors such as seasonal trends and regional economic conditions (Powell, 2007; Gijsbrechts et al., 2022). Similar factored discrete structure arises in materials process optimization (Wu and Hamada, 2011), multi-component maintenance scheduling (De Jonge and Scarf, 2020), network routing, and resource allocation.

When learning must proceed online through direct interaction with the environment, sample efficiency becomes critical. The curse of dimensionality renders classical tabular methods impractical (Bellman, 1957; Szepesvari, 2010; Powell, 2007), as each interaction may be costly or risky. These considerations highlight the need for approximation methods that are both expressive and statistically efficient (Gheshlaghi Azar et al., 2013; Sam et al., 2023).

Classical approaches range from tabular Q-learning (Watkins and Dayan, 1992) to linear function approximation (Bradtke and Barto, 1996) and deep neural networks such as DQN (Mnih et al., 2015) and SAC (Christodoulou, 2019). While deep RL methods offer representational flexibility, they typically require extensive samples and do not explicitly exploit the multi-dimensional structure inherent in discretized state-action spaces, motivating structured alternatives.

Low-rank structure offers a principled alternative that addresses both sample efficiency and structural exploitation. A line of theoretical work has established that when the underlying MDP admits low-rank structure, sample complexity can be fundamentally reduced from scaling with the product of state and action space sizes to scaling with their sum (Jiang et al., 2017; Agarwal et al., 2020; Uehara et al., 2022). This theoretical insight motivates methods that learn compact value function representations. Matrix-based approaches re-

duce parameters via SVD or nuclear-norm regularization (Shah et al., 2020), and recent model-free methods such as LoRa-VI achieve finite-sample guarantees through structured estimation (Stojanovic et al., 2024a; Modi et al., 2024). Tensor decomposition further extends this idea: by representing the Q-function as a multi-dimensional array with CP factorization, tensor methods reduce complexity from exponential to linear in the number of dimensions while preserving mode-wise interactions that matrix flattening discards (Tsai et al., 2021; Rozada et al., 2024).

However, existing tensor-based Q-learning focuses on representation fidelity rather than sample efficiency, employing standard ε -greedy exploration without exploiting structural uncertainty. Matrix-based methods with sample-efficiency guarantees, conversely, do not extend naturally to multi-dimensional state-action representations. To the best of our knowledge, no existing method combines low-rank tensor structure with uncertainty-aware exploration for sample-efficient online learning.

Based on this motivation, we propose Tensor-Efficient Q-Learning (TEQL), an online, model-free reinforcement learning framework that takes advantage of the low-rank tensor structure and uncertainty-aware exploration to improve the statistical efficiency of value-function estimation in high-dimensional settings. Our approach makes three main contributions.

First, we develop a low-rank tensor Q-learning scheme with frequency-based regularization that compresses the value-function representation from exponential to linear complexity in the number of dimensions. We establish convergence in expectation to a neighborhood of the optimal Q-function under a low-rank structural assumption, with the radius explicitly separating approximation and stochastic error components.

Second, we propose Error-Uncertainty Guided Exploration (EUGE), an uncertainty-aware action-selection rule that augments value estimates with a bonus based on decomposition

error and visit counts. By tracking how rapidly the tensor approximation changes across iterations, EUGE prioritizes state-action pairs whose estimates remain uncertain and helps allocate samples more effectively in high-dimensional spaces.

Third, we provide empirical evaluations, including ablation and sensitivity studies, demonstrating that TEQL improves sample efficiency relative to tensor and non-tensor baselines under the same interaction budget. Across classical control environments, TEQL achieves faster improvement in returns and more rapid reduction of value-function error, and we examine how its performance varies with tensor rank, discretization levels, and exploration parameters.

2 Preliminaries

We review Q -learning, low-rank value function representations, and structural assumptions that support the TEQL framework. We also specify the notation used throughout this paper. Scalars use lowercase letters (e.g., q, r, γ), vectors use bold lowercase (e.g., $\mathbf{s}, \mathbf{a}, \mathbf{f}$), matrices use bold uppercase (e.g., \mathbf{Q}, F), and tensors use calligraphic letters (e.g., \mathcal{Q}, \mathcal{T}). Sets use calligraphic letters (e.g., \mathcal{S}, \mathcal{A}); $|\mathcal{S}|$ and $|\mathcal{A}|$ denote the cardinalities of the discretized state and action spaces, respectively. The optimal Q -function is q^* , and $\hat{\mathcal{Q}}$ denotes the low-rank tensor approximation. Rank- R refers to the CP rank of the low-rank tensor. Factor matrices are F_n with time-indexed versions $F_n^{(t)}$. Transition and reward functions use \mathcal{P} and \mathcal{R} .

The method developed in this paper primarily targets MDPs with discrete, factored state-action spaces, where each dimension of the state and action takes values from a finite set. This discrete structure is inherent in the application domains discussed in Section 1, including clinical treatment optimization, inventory management, and maintenance scheduling. Many high-dimensional control tasks exhibit value functions with low-rank tensor struc-

ture, where state and action variables interact through a limited number of latent factors. Tensor decomposition provides a natural way to exploit this structure, and discrete indexing is the mechanism through which the factored state-action components are represented and compressed. Although continuous state-action spaces are not the primary target of this method, TEQL can still be applied to such settings by discretizing each continuous dimension into a finite set of bins prior to learning, which is a common practice in Q-learning. The approximation error introduced by this discretization step is absorbed into the constant B_R analyzed in Section 2.2.

2.1 Low-Rank Value Function Representations for Q-Learning

A discounted Markov Decision Process (MDP) is defined by the tuple $\langle \mathcal{S}, \mathcal{A}, \mathcal{P}, \mathcal{R}, \gamma \rangle$. For a state s and action a , the optimal Q-function satisfies

$$q^*(s, a) = \mathbb{E}[r + \gamma \max_{a'} q^*(s', a') \mid s, a]. \quad (1)$$

Q-learning updates the estimate $q(s, a)$ as

$$q(s, a) \leftarrow q(s, a) + \alpha(r + \gamma \max_{a'} q(s', a') - q(s, a)). \quad (2)$$

Tabular updates become infeasible in high-dimensional spaces, so compact representations such as low-rank matrix or tensor models are required.

The Q-function can be arranged as a matrix $\mathbf{Q} \in \mathbb{R}^{C_S \times C_A}$ or as a tensor when the state and action contain multiple components. For high-dimensional state-action spaces, a tensor representation preserves the multiway structure.

Let $s \in \mathbb{R}^{D_S}$ and $a \in \mathbb{R}^{D_A}$ denote underlying continuous state and action variables when applicable. After discretization, the combined index vector (i_1, \dots, i_N) with $N = D_S + D_A$ identifies one tensor entry. This discretized representation naturally induces a multi-

dimensional tensor form of the Q-function, given by

$$Q \in \mathbb{R}^{d_1 \times \dots \times d_N}. \quad (3)$$

The discretization levels determine the mode sizes (d_1, \dots, d_N) . The total number of discretized states is $|\mathcal{S}| = \prod_{n=1}^{D_S} d_n$, which grows exponentially with dimension D_S . This exponential growth motivates the use of low-rank parameterizations that scale as $O(R \sum_n d_n)$ rather than $O(|\mathcal{S}|)$.

The CP (CANDECOMP/PARAFAC) decomposition represents a tensor as a sum of rank-one components, providing a compact parameterization when the tensor admits low-rank structure. The specific formulation and computational details are presented in Section 3.1, where we describe how TEQL maintains and updates this representation during learning.

In related low-rank reinforcement learning formulations, additional regularity conditions such as coherence or spikiness are often used to formalize when value-function structure can be recovered from limited observations; our analysis here is stated directly in terms of CP approximability.

Having established the representational form and parameterization, we next specify the structural assumption that links this model class to the optimal Q-function.

2.2 Structural Assumptions for Tensor Value Functions

The tensor representation defined above describes a compact model class for approximating value functions in high-dimensional MDPs. To ensure that this representation supports effective learning, we specify a structural condition on the optimal Q-function Q^* . This assumption constrains how well Q^* can be approximated within the class of rank- R CP tensors.

Assumption 1 (Low-rank CP Approximability). *For a given rank parameter R , the op-*

imal value tensor Q^* admits a rank- R CP approximation up to residual error B_R , in the sense that

$$\inf_{\text{rank}_{\text{CP}}(Q) \leq R} \|Q - Q^*\|_{\infty} \leq B_R. \quad (4)$$

Assumption 1 does not require that Q^* be exactly low rank. Rather, it states that Q^* can be well approximated by a rank- R CP tensor, with the approximation error absorbed into the constant B_R . This is analogous to low-rank approximations widely used in multivariate analysis, where the dominant structure of a high-dimensional function can often be captured by a small number of multiplicative components even though the true function is not strictly separable. We emphasize that this assumption concerns the value function Q^* , not the state-action space itself. The assumption concerns the value function mapping, not the dimensionality of the state or action spaces.

A low-rank approximation is particularly plausible in environments where the state and action variables interact through a moderate number of latent or weakly coupled factors. Examples include settings with approximately separable physical effects, smooth dependencies across dimensions, or dynamics that evolve on a lower-dimensional manifold embedded in the ambient space. In such cases, the dominant variation in Q^* can often be represented with a limited number of rank-one tensor components, leading to a small B_R .

Conversely, when interactions across dimensions are highly entangled or exhibit strong discontinuities, the approximation error B_R may remain non-negligible for any feasible rank R . This reflects a design trade-off: the approximation error B_R can be systematically reduced by increasing the tensor rank R , albeit at the cost of increased computational complexity.

Assumption 1 requires only that there exist mode sizes (d_1, \dots, d_N) and a rank R such that the approximation error B_R is bounded. The theoretical guarantees in Section 3.4 do not impose additional restrictions on these quantities. In practice, we choose (d_1, \dots, d_N) and R

so that the parameter count $R \sum_{n=1}^N d_n$ is much smaller than the full tensor size $\prod_{n=1}^N d_n$, preserving the computational and statistical advantages of the low-rank representation while allowing any residual approximation error to be absorbed into B_R .

3 Methodology

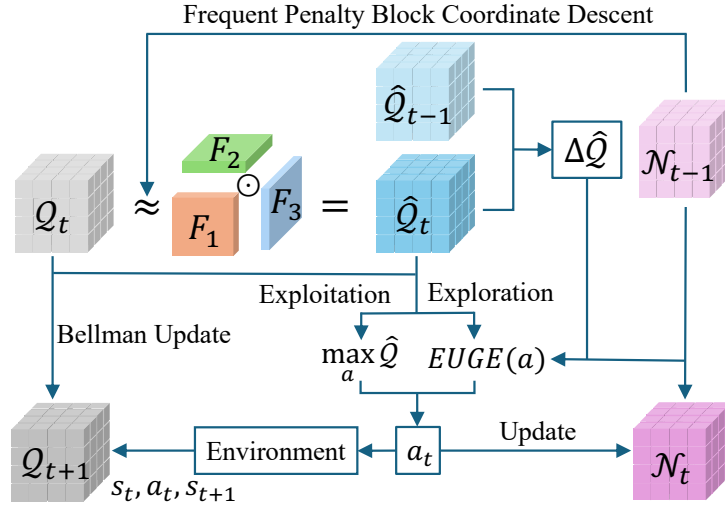


Figure 1: Framework of the Tensor-Efficient Q -Learning (TEQL) Algorithm.

Figure 1 summarizes the Tensor-Efficient Q -Learning (TEQL) framework. The algorithm maintains a low-rank CP approximation \hat{Q}_t and iterates through three stages: action selection via EUGE, environment interaction, and tensor update via frequency-regularized block coordinate descent. The decomposition error ΔQ_t and visit counts \mathcal{N}_t are carried forward to guide subsequent exploration, forming a closed loop.

At time step t , the algorithm starts from the previous estimate \hat{Q}_{t-1} , represented by a rank- R CP decomposition with factor matrices $\{F_n^{(t-1)}\}_{n=1}^N$. Given the current state s_t , an action a_t is selected using the Error-Uncertainty Guided Exploration (EUGE) mechanism, which combines the estimated value $\hat{Q}_{t-1}(s_t, a)$ with an exploration bonus derived from visit counts and approximation changes.

After executing a_t , the agent observes a reward r_t and next state s_{t+1} , forming a transition tuple (s_t, a_t, r_t, s_{t+1}) . The tuple and the previous estimate \hat{Q}_{t-1} are used to update the approximation by solving a frequency-regularized tensor decomposition problem via block coordinate descent, yielding an updated estimate \hat{Q}_t .

The change between successive approximations, $\Delta Q_t(s_t, a_t) = |\hat{Q}_t(s_t, a_t) - \hat{Q}_{t-1}(s_t, a_t)|$, is recorded together with the updated visit counts \mathcal{N}_t . These quantities are carried forward to guide subsequent action selection through EUGE. Throughout, the CP rank is denoted by R , and the index $r \in \{1, \dots, R\}$ is used only as a summation index within the decomposition.

3.1 Low-Rank Tensor Q-Function Update with Frequency Regularization

TEQL approximates the Q-function as a low-rank tensor $\hat{Q}_t \in \mathbb{R}^{d_1 \times \dots \times d_N}$, where each mode corresponds to one discretized state or action component and $N = D_S + D_A$ is the total number of state and action dimensions. The CP (CANDECOMP/PARAFAC) decomposition represents this tensor as a sum of rank-one components. For an index tuple (i_1, \dots, i_N) , the CP representation is

$$\hat{Q}_t(i_1, \dots, i_N) = \sum_{r=1}^R \prod_{n=1}^N F_n^{(t)}(i_n, r),$$

where $F_n^{(t)} \in \mathbb{R}^{d_n \times R}$ are factor matrices at time t . This parameterization reduces the number of parameters from $\prod_{n=1}^N d_n$ in a tabular representation to $R \sum_{n=1}^N d_n$, which we denote by d_{eff} for subsequent analysis.

TEQL builds on a baseline tensor Q-learning update (Rozada et al., 2024), which minimizes squared temporal-difference error at observed pairs. In particular, given (s_t, a_t, r_t, s_{t+1}) , the baseline corresponds to optimizing a local per-sample objective of the form

$$\min_Q \left(q_t^{\text{target}}(s_t, a_t) - Q(s_t, a_t) \right)^2. \quad (5)$$

This baseline can put most weight on frequently visited state-action pairs and may allocate fewer updates to rarely visited pairs.

To adjust the allocation of updates, TEQL introduces a frequency-based regularization term, drawing on the principle of visit-count weighting from (Auer et al., 2002; Jaksch et al., 2010). At time t the update solves

$$\begin{aligned} \min_{\{\hat{Q}_t^{(n)}\}_{n=1}^N} & \left[(q_t^{\text{target}}(s_t, a_t) - \hat{Q}_t(s_t, a_t))^2 - \lambda \frac{\hat{Q}_t(s_t, a_t)^2}{\mathcal{N}_{t-1}(s_t, a_t) + \epsilon} \right], \\ \text{s.t.} \quad \hat{Q}_t &= \sum_{r=1}^R F_1^{(t)}(\cdot, r) \circ F_2^{(t)}(\cdot, r) \circ \dots \circ F_N^{(t)}(\cdot, r). \end{aligned} \quad (6)$$

where $q_t^{\text{target}}(s_t, a_t) = r_t + \gamma \max_{a'} \hat{Q}_{t-1}(s_{t+1}, a')$ is the target value, $\lambda > 0$ controls the regularization strength, $\epsilon > 0$ avoids division by zero, and $\mathcal{N}_{t-1}(s_t, a_t)$ is the visit count of (s_t, a_t) before time t .

We use the squared TD error to form a differentiable objective suitable for gradient-based block coordinate descent. The per-sample loss combining squared TD error and frequency regularization is

$$L_{s_t, a_t} = \frac{1}{2} \left(q_t^{\text{target}}(s_t, a_t) - \hat{Q}_t(s_t, a_t) \right)^2 - \lambda \frac{\hat{Q}_t(s_t, a_t)^2}{\mathcal{N}_{t-1}(s_t, a_t) + \epsilon}. \quad (7)$$

The regularization term introduces frequency-dependent regularization. Unlike standard ℓ_2 regularization that uniformly shrinks values toward zero, this term interacts with the temporal-difference term in a direction-dependent manner. To see this, note that the derivative of (7) with respect to \hat{Q}_t is

$$\frac{\partial L_{s_t, a_t}}{\partial \hat{Q}_t} = -(q_t^{\text{target}} - \hat{Q}_t) - \frac{2\lambda \hat{Q}_t}{\mathcal{N}_{t-1} + \epsilon},$$

where we abbreviate $q_t^{\text{target}} = q_t^{\text{target}}(s_t, a_t)$, $\hat{Q}_t = \hat{Q}_t(s_t, a_t)$, and $\mathcal{N}_{t-1} = \mathcal{N}_{t-1}(s_t, a_t)$. When \hat{Q}_t is positive and exceeds the target (overestimation), the first term is positive and pushes \hat{Q}_t downward via gradient descent, while the second term is negative and resists

this correction. The two terms act in opposite directions, making the update conservative. When \hat{Q}_t is below the target (underestimation), both terms are negative and align in the same direction, allowing the correction to proceed unimpeded. The coefficient $1/(\mathcal{N}_{t-1} + \epsilon)$ modulates the strength of this direction-dependent effect: at frequently visited pairs where \mathcal{N}_{t-1} is large, the regularization term is negligible and TD learning dominates; at rarely visited pairs where \mathcal{N}_{t-1} is small, the regularization effect is pronounced, providing stronger resistance to overestimation while not impeding underestimation corrections. Since overestimation induced by the maximization operator is a primary source of instability in Q-learning (Thrun and Schwartz, 1993; Van Hasselt et al., 2016), this mechanism is particularly valuable at sparsely visited state-action pairs where such bias is most likely to occur. In summary, at frequently visited pairs, the regularization coefficient is small and TD learning dominates with moderate update magnitudes. At rarely visited pairs, the regularization coefficient is large and the direction-dependent effect becomes significant: overestimation is dampened, while underestimation triggers accelerated correction. This is desirable because rarely visited pairs are precisely where estimates are most uncertain and require larger updates when underestimated.

While this mechanism does not directly promote exploration, it shapes the distribution of ΔQ_t and subsequently affects exploration behavior through the EUGE strategy described in Section 3.2.

For each observed pair, the decomposition error is defined as

$$\Delta Q_t(s_t, a_t) = |\hat{Q}_t(s_t, a_t) - \hat{Q}_{t-1}(s_t, a_t)|. \quad (8)$$

This quantity is distinct from the TD error and reflects the change induced by the tensor update. EUGE uses this decomposition error to construct an exploration bonus.

The gradient of (7) with respect to a factor entry $F_n(i_n, r)$ is

$$\begin{aligned} \nabla_{F_n(i_n, r)} L_{s_t, a_t} = & - \left(q_t^{\text{target}}(s_t, a_t) - \hat{Q}_t(s_t, a_t) \right) \prod_{m \neq n} F_m(i_m, r) \\ & - 2\lambda \frac{\hat{Q}_t(s_t, a_t)}{\mathcal{N}_{t-1}(s_t, a_t) + \epsilon} \prod_{m \neq n} F_m(i_m, r). \end{aligned} \quad (9)$$

During this computation, $q_t^{\text{target}}(s_t, a_t)$ is treated as a constant because it is defined using \hat{Q}_{t-1} from the previous step. Only $\hat{Q}_t(s_t, a_t)$ depends on the current factor matrices.

At each time step t , the factor matrices $F_n^{(t-1)}$ are used to initialize the current optimization variables, denoted by F_n , which are updated in-place during the inner block coordinate descent and recorded as $F_n^{(t)}$ upon completion. The factor matrices F_n are updated by gradient descent:

$$F_n(i_n, r) \leftarrow F_n(i_n, r) - \alpha_t \nabla_{F_n(i_n, r)} L_{s_t, a_t}, \quad (10)$$

where α_t is a step size. Updates proceed until the change in $\hat{Q}_t(s_t, a_t)$ is below a threshold or a maximum number of iterations is reached.

Algorithm 1 summarizes the low-rank tensor Q-function update.

3.2 Error-Uncertainty Guided Exploration (EUGE)

The tensor update produces ΔQ_t , which quantifies estimation uncertainty beyond visit counts alone. EUGE leverages this signal for action selection: At time t , for each action a in state s_t , EUGE defines

$$\text{EU}_t(s_t, a) = \hat{Q}_{t-1}(s_t, a) + c \left(\Delta Q_{t-1}(s_t, a) + \sqrt{\frac{\log \mathcal{N}_{\text{total}, t-1}(s_t)}{\mathcal{N}_{t-1}(s_t, a) + 1}} \right), \quad (11)$$

where $\mathcal{N}_{t-1}(s_t, a)$ is the visit count of (s_t, a) , $\mathcal{N}_{\text{total}, t-1}(s_t) = \sum_a \mathcal{N}_{t-1}(s_t, a)$ is the total visits to s_t , and $c > 0$ is an exploration parameter. The action is chosen as

$$a_t = \arg \max_a \text{EU}_t(s_t, a).$$

Algorithm 1 Low-Rank Tensor Q-Function Update

- 1: **Input:** State s_t , action a_t , reward r_t , next state s_{t+1} , Q-function \hat{Q}_{t-1} , factor matrices $F_n^{(t-1)}$, visit count $\mathcal{N}_{t-1}(s_t, a_t)$, error tensor ΔQ_{t-1} , regularization parameter λ , regularization term constant ϵ , learning rate parameters α_0, κ , time step t , threshold τ , maximum inner iterations I_{\max} .
 - 2: Set step size $\alpha_t = \alpha_0 / (1 + \kappa t)$.
 - 3: Compute target value $q_t^{\text{target}}(s_t, a_t) = r_t + \gamma \max_{a'} \hat{Q}_{t-1}(s_{t+1}, a')$. $\triangleright q_t^{\text{target}}$ depends only on \hat{Q}_{t-1} and is fixed during the inner updates.
 - 4: **for** $n = 1, \dots, N$ **do**
 - 5: Fix $F_m^{(t-1)}$ for all $m \neq n$.
 - 6: Set $\hat{Q}_{\text{prev}} = \hat{Q}_{t-1}(s_t, a_t)$.
 - 7: **for** $i = 1$ to I_{\max} **do**
 - 8: Define the local loss at (s_t, a_t) : $L_{s_t, a_t} = \frac{1}{2} (q_t^{\text{target}}(s_t, a_t) - \hat{Q}_t(s_t, a_t))^2 - \lambda \frac{\hat{Q}_t(s_t, a_t)^2}{\mathcal{N}_{t-1}(s_t, a_t) + \epsilon}$,
 where q_t^{target} and \mathcal{N}_{t-1} are treated as constants when updating F_n , while \hat{Q}_t changes through F_n .
 - 9: Compute gradient $\nabla_{F_n(i_n, r)} L_{s_t, a_t}$ as in (9).
 - 10: Update $F_n(i_n, r) \leftarrow F_n(i_n, r) - \alpha_t \nabla_{F_n(i_n, r)} L_{s_t, a_t}$.
 - 11: Recompute $\hat{Q}_{\text{curr}} = \hat{Q}_t(s_t, a_t)$.
 - 12: **if** $|\hat{Q}_{\text{curr}} - \hat{Q}_{\text{prev}}| < \tau$ **then**
 - 13: **break**
 - 14: **end if**
 - 15: $\hat{Q}_{\text{prev}} = \hat{Q}_{\text{curr}}$.
 - 16: **end for**
 - 17: **end for**
 - 18: Set $F_n^{(t)} = F_n$.
 - 19: Update $\hat{Q}_t(s, a) = \sum_{r=1}^R \prod_{n=1}^N F_n^{(t)}(i_n, r)$.
 - 20: Set $\Delta Q_t(s_t, a_t) = |\hat{Q}_t(s_t, a_t) - \hat{Q}_{t-1}(s_t, a_t)|$.
 - 21: Update visit count $\mathcal{N}_t(s_t, a_t) = \mathcal{N}_{t-1}(s_t, a_t) + 1$.
 - 22: **Output:** $\hat{Q}_t, F_n^{(t)}, \Delta Q_t, \mathcal{N}_t$.
-

The EUGE value combines the current tensor estimate $\hat{Q}_{t-1}(s_t, a)$, the decomposition error $\Delta Q_{t-1}(s_t, a)$, and a visit-count-based bonus. Larger decomposition error or smaller visit count yields a larger bonus, prioritizing actions whose Q-value estimates are either changing rapidly or have been sampled infrequently. Algorithm 2 summarizes EUGE. The form of the bonus follows the standard UCB principle of favoring uncertain actions, with the additional decomposition-error term reflecting uncertainty induced by low-rank approximation rather than visitation alone.

Algorithm 2 Error-Uncertainty Guided Exploration (EUGE)

- 1: **Input:** State s_t , tensor Q-function \hat{Q}_{t-1} , factor matrices $F_n^{(t-1)}$, error tensor ΔQ_{t-1} , visit counts \mathcal{N}_{t-1} , parameter c .
 - 2: Initialize possible actions $\mathcal{A}_{\text{possible}}$.
 - 3: **for** each $a \in \mathcal{A}_{\text{possible}}$ **do**
 - 4: Compute $\hat{Q}_{t-1}(s_t, a)$ using $F_n^{(t-1)}$.
 - 5: Compute $\text{bonus}_t(s_t, a) = \Delta Q_{t-1}(s_t, a) + \sqrt{\frac{\log \mathcal{N}_{\text{total}, t-1}(s_t)}{\mathcal{N}_{t-1}(s_t, a) + 1}}$.
 - 6: Set $\text{EU}_t(s_t, a) = \hat{Q}_{t-1}(s_t, a) + c \cdot \text{bonus}_t(s_t, a)$.
 - 7: **end for**
 - 8: Select $a_t = \arg \max_a \text{EU}_t(s_t, a)$.
 - 9: **Output:** a_t .
-

3.3 Complete TEQL Algorithm and Model Configuration

The TEQL framework integrates the low-rank tensor update (Algorithm 1) and the EUGE exploration strategy (Algorithm 2) into an online learning loop. At each time step, the agent uses EUGE to select an action based on the current Q-function estimate and uncertainty measures, observes the resulting transition, and then updates the tensor factors via block coordinate descent. The decomposition error ΔQ_t computed during the update step feeds back into the EUGE bonus for subsequent action selection, creating a coupling between

representation learning and exploration.

TEQL operates in an infinite-horizon discounted Markov Decision Process defined by $\langle \mathcal{S}, \mathcal{A}, \mathcal{P}, \mathcal{R}, \gamma \rangle$, where \mathcal{S} and \mathcal{A} are the state and action spaces, \mathcal{P} is the transition kernel, \mathcal{R} is the reward function, and $\gamma \in (0, 1)$ is the discount factor. The algorithm runs for T episodes, each consisting of H steps. Algorithm 3 presents the complete procedure. The computational complexity of TEQL’s tensor update via block coordinate descent is $\mathcal{O}(NRI_{\max})$ per update, where N is the tensor order, R the rank, and I_{\max} the maximum inner iterations. Memory usage is $\mathcal{O}(d_{\text{eff}})$, as defined in Section 3.1.

Algorithm 3 involves several quantities that control the learning process. We organize them into three categories and provide general selection guidelines below; the specific values used in our experiments are reported in Section 4.1.

Model-capacity parameters. The discretization levels (d_1, \dots, d_N) and the tensor rank R must be specified before running TEQL. These quantities determine the tensor shape of \hat{Q} and the parameter count $R \sum_{n=1}^N d_n$, which governs the statistical and computational complexity of estimating the tensor factors and appears explicitly in the error bounds in Section 3.4. TEQL does not adaptively modify (d_1, \dots, d_N) or R during learning; both are fixed hyperparameters chosen prior to training. When state or action variables arise from continuous domains, each dimension is mapped to a finite set of indices through uniform binning. The number of bins d_n is selected so that (i) the discretization covers the full admissible range of that dimension, and (ii) the resulting discrete state-action space remains compatible with available computation. This procedure does not require environment-specific domain knowledge; the same uniform binning scheme applies across different tasks. The tensor rank R is chosen to satisfy $R \sum_{n=1}^N d_n \ll \prod_{n=1}^N d_n$, so that the low-rank representation yields a substantial reduction in the number of parameters relative to a full tabular representation. Because the intrinsic CP rank of Q^* and the

Algorithm 3 Tensor-Efficient Q-Learning (TEQL)

- 1: **Input:** Discount factor γ , tensor rank R , regularization parameter λ , regularization constant ϵ , learning rate parameters α_0, κ , exploration constant c , convergence threshold τ , maximum inner iterations I_{\max} , number of episodes T , episode length H .
 - 2: Initialize factor matrices $F_n^{(0)} \in \mathbb{R}^{d_n \times R}$ for $n = 1, \dots, N$.
 - 3: Initialize Q-function $\hat{Q}_0(s, a) = \sum_{r=1}^R \prod_{n=1}^N F_n^{(0)}(i_n, r)$.
 - 4: Initialize visit counts $\mathcal{N}_0(s, a) = 0$ for all (s, a) .
 - 5: Initialize error tensor $\Delta Q_0(s, a) = 0$ for all (s, a) .
 - 6: **for** episode $e = 1, \dots, T$ **do**
 - 7: Observe initial state s_1 from environment.
 - 8: **for** step $h = 1, \dots, H$ **do**
 - 9: Select action a_h using EUGE (Algorithm 2) with inputs $(s_h, \hat{Q}, F_n, \Delta Q, \mathcal{N}, c)$.
 - 10: Execute a_h , observe reward r_h and next state s_{h+1} .
 - 11: Update $(\hat{Q}, F_n, \Delta Q, \mathcal{N})$ using Low-Rank Tensor Update (Algorithm 1) with inputs $(s_h, a_h, r_h, s_{h+1}, \hat{Q}, F_n, \mathcal{N}, \Delta Q, \lambda, \epsilon, \alpha_0, \kappa, t, \tau, I_{\max})$, where $t = (e - 1)H + h$.
 - 12: **end for**
 - 13: **end for**
 - 14: **Output:** Learned Q-function \hat{Q} , factor matrices F_n .
-

approximation error B_R are generally unknown, R is treated as a tunable parameter. We select R following prior work on low-rank value-function approximation, where moderate ranks are commonly used to balance approximation accuracy and parameter efficiency. In the experimental section, we report sensitivity results across different discretization levels while keeping R fixed, in order to isolate the effect of discretization and assess robustness. This configuration procedure specifies a complete and fixed tensor model class prior to training. The structural assumption in Section 2.2 determines whether this model class admits a sufficiently accurate approximation of Q^* . If the approximation error B_R is large, this limitation appears as a non-negligible approximation bias in the neighbourhood radius of Theorem 1 and in the finite-sample error behaviour discussed in Section 3.4.

Numerical optimization parameters. Four parameters govern the optimization dynamics of the block coordinate descent. The initial learning rate α_0 controls the step size of Q-value updates; values that are too large cause divergence, while values that are too small slow convergence. The decay coefficient κ in the schedule $\alpha_t = \alpha_0 / (1 + \kappa t)$ ensures asymptotic convergence; standard choices from the stochastic approximation literature apply. The convergence threshold τ for inner iterations terminates the block coordinate descent when the change in $\hat{Q}_t(s_t, a_t)$ falls below τ ; in practice, early termination typically occurs within 5 to 10 iterations. An optional parameter I_{\max} can be used to cap the number of inner iterations when computational cost is a concern. The smoothing constant ϵ in the regularization term prevents division by zero when visit counts are small; any value that is negligible relative to typical visit counts suffices. Within a broad range, moderate changes to these parameters affect convergence speed but not asymptotic performance.

Algorithm-specific hyperparameters. Two hyperparameters directly influence TEQL’s exploration and regularization behavior. The frequency regularization strength λ controls the intensity of the visit-count-dependent regularization in (6). Larger λ provides stronger

resistance to value changes at sparsely visited pairs, counteracting overestimation but potentially slowing convergence. In practice, λ should be small enough to preserve TD learning dynamics while providing measurable stabilization. The exploration coefficient c in the EUGE bonus (11) scales the exploration bonus. This parameter should be calibrated so that the exploration bonus is commensurate with the range of Q-values in the problem; if typical values lie in $[0, V_{\max}]$, then c of order $O(1)$ to $O(V_{\max})$ is appropriate. Both λ and c can be calibrated on a single representative environment using early-stage learning curves and then held fixed across all experiments. Section 4.5 reports sensitivity analysis demonstrating robustness within a broad range around the chosen values.

3.4 Theoretical Guarantees

This section provides theoretical support for TEQL that formalizes the design choices in Sections 2-3. Rather than aiming for exact optimality guarantees, our goal is to understand how approximation, regularization, and exploration interact to produce stable and efficient learning behavior in high-dimensional settings.

Assumption 1 (Low-rank CP Approximability) has already been introduced in Section 2.2. It characterizes the expressive power of the rank- R tensor class and captures the irreducible modeling bias through the constant B_R . Here we impose only a standard boundedness condition, which can be enforced in practice by factor clipping or projection in the CP parameterization.

Assumption 2 (Bounded Iterates). *The TEQL iterates remain uniformly bounded:*

$$\|\hat{Q}_t\|_\infty \leq V_{\max} \text{ for all } t \geq 0.$$

This assumption ensures that all iterates stay within a compact region where the approximation error characterized by Assumption 1 remains meaningful and where the Bellman operator is well behaved.

We state the convergence result in interpretable form; the detailed recursion is deferred to the appendix.

Theorem 1 (Convergence to a Neighborhood). *Under Assumptions 1 and 2, TEQL converges to a neighborhood of the optimal Q-function q^* in expected supremum norm. The asymptotic error decomposes into two irreducible components: (i) an approximation bias determined by B_R from Assumption 1, and (ii) a stochastic component induced by using the single-sample TD target (6).*

A finite-time bound with explicit error decomposition is given in Appendix A.1. Theorem 1 shows that TEQL behaves like a contractive Bellman-type iteration (due to $\gamma \in (0, 1)$), but cannot converge exactly to q^* unless (i) the rank- R class is expressive enough (B_R small), and (ii) TD noise vanishes. This result clarifies the fundamental performance limit of TEQL: stability and accuracy are achieved up to unavoidable approximation and sampling effects, rather than through exact Bellman fixed-point recovery. In other words, TEQL is stable and accurate up to the modeling error B_R and the inherent sampling noise.

Having established that TEQL converges in a controlled manner, we next examine how the algorithm allocates its updates across the state-action space.

The regularizer in (7) introduces a visit-count-dependent term in the gradient. Proposition 1 establishes an upper bound on the update magnitude $|\Delta Q_t(s_t, a_t)|$ that includes a component scaling as $1/(\mathcal{N}_{t-1}(s_t, a_t) + \epsilon)$. This bound is tighter at frequently visited pairs, reflecting that the regularization effect diminishes with increasing visit count.

Proposition 1 (Frequency-Regularized Update Shrinkage). *Under Assumption 2, the magnitude of the one-step value change $\Delta Q_t(s_t, a_t)$ admits an upper bound consisting of a base term (depending on the step size and boundedness constants) plus an additional term that decays on the order of $1/(\mathcal{N}_{t-1}(s_t, a_t) + \epsilon)$. Consequently, for a fixed step-size schedule,*

updates at frequently visited pairs become progressively smaller.

The detailed proof is given in Appendix A.2. This result formalizes how the upper bound on update magnitude varies with visitation frequency. At frequently visited pairs, the bound is tighter, reflecting that TD learning dominates with minimal regularization interference. At rarely visited pairs, the bound is looser, but as shown in Section 3.1, the direction-dependent nature of the regularization selectively dampens overestimation while allowing underestimation corrections.

We now analyze the selection rule (11). Because EUGE explicitly depends on both visit counts and decomposition error, the update shrinkage property in Proposition 1 plays a direct role in the exploration dynamics. Importantly, we do not introduce any new exploration score: we use exactly $EU_t(s, a)$ as defined in Section 3.2. The main takeaway is that EUGE does not keep choosing actions that are simultaneously (i) clearly worse than the best action at the current state and (ii) already low-uncertainty according to the bonus terms in (11).

Proposition 2 (Logarithmic Re-Selection of Suboptimal Low-Uncertainty Actions). *Fix a state s . Consider an action a such that, after some time, its estimated value $\hat{Q}_{t-1}(s, a)$ remains separated below the best estimated action at s by a fixed positive margin, while its EUGE bonus in (11) becomes small due to (i) small decomposition error $\Delta Q_{t-1}(s, a)$ and (ii) a growing visit count $\mathcal{N}_{t-1}(s, a)$. Then EUGE selects a only a logarithmic number of times as the horizon increases.*

The proof is provided in Appendix A.3. Together, Theorem 1 and Propositions 1-2 provide a coherent explanation of TEQL: convergence ensures that learning stabilizes near an optimal solution, frequency regularization governs how updates are distributed across the state-action space, and EUGE leverages both effects to guide exploration. (i) stable learning up

to approximation bias B_R and TD noise, (ii) computational effort automatically reallocated away from frequent pairs by frequency regularization, and (iii) exploration guided by ΔQ_t and visit counts avoids repeatedly sampling actions that are both unpromising and already well-estimated.

4 Numerical Study

This section tests whether tensor low-rank structure improves sample efficiency when all methods are constrained to the same parameter budget. We evaluate on three environments with increasing state-action complexity, namely Pendulum ($D_S = 2, D_A = 1$), CartPole ($D_S = 4, D_A = 1$), and Highway ($D_S = 9, D_A = 1$). These environments are selected because their Q -functions admit accurate low-rank approximations; singular value analysis in [Rozada et al. \(2024\)](#) shows that rank-10 (Pendulum, Cartpole) and rank-20 (Highway) tensors capture over 90% of spectral energy under comparable discretization schemes.

To isolate the effect of algorithmic design from model capacity, all methods operate on identical discretized MDPs and are matched to the same order of magnitude in trainable parameters. This parameter-matched design is central to our evaluation because tensor methods are specifically intended for learning in regimes where model capacity is limited. We constrain all methods to equivalent budgets, specifically 500 for Pendulum, 700 for CartPole ($R = 10$), and 3,700 for Highway ($R = 20$), to directly test whether tensor low-rank structures provide a meaningful advantage. These budgets are deliberately set below typical deep learning scales to focus the evaluation on the intrinsic parameter efficiency of each architecture.

Baselines include (i) TLR ([Rozada et al., 2024](#)), which shares TEQL’s CP representation but uses ϵ -greedy exploration without regularization, (ii) LoRa-VI, adapted from the matrix low-rank framework of [Stojanovic et al. \(2024b\)](#) to the Q-learning setting, and (iii) DQN

(Mnih et al., 2015) and discrete SAC (Christodoulou, 2019). We include LoRa-VI not as a direct competitor but to illustrate the limitations of matrix-based low-rank methods in online trajectory-based learning: the original framework assumes uniform or leverage-score-guided sampling for matrix completion, whereas online RL produces correlated, non-uniform data that violates these assumptions. All methods receive discretized bucket indices as input and output Q -values over the finite action set. DQN and SAC are compressed to the same parameter scale by reducing hidden layer widths; SAC further distributes its budget across actor, critic, and temperature networks, leaving each component with fewer parameters than a single DQN network of equivalent total size. Detailed architectures for all methods are provided in Appendix B.

4.1 Hyperparameter Configuration

Table 1 reports the complete hyperparameter configuration for each environment. The discretization column lists the number of bins per dimension in the order they appear in the state-action vector; for example, CartPole has five dimensions discretized into 10, 10, 20, 20, and 10 bins respectively, and Highway has nine state dimensions each with 20 bins and one action dimension with 5 bins. The numerical optimization parameters ($\alpha_0, \kappa, \tau, \epsilon$) were set following standard heuristics from the Q-learning and tensor factorization literature. The algorithm-specific hyperparameters (λ, c) were calibrated on CartPole using early-stage learning curves and then held fixed across all environments. The sensitivity analysis in Section 4.5 demonstrates robustness within a broad range around these values. Results aggregate 100 independent runs, and shaded regions show mean \pm standard deviation.

Table 1: Hyperparameter settings for all environments.

Category	Parameter	Pendulum	CartPole	Highway
Model capacity	Tensor rank R	10	10	20
	Bins per dimension (d_1, \dots, d_N)	(20, 20, 10)	(10, 10, 20, 20, 10)	$(20 \times 9, 5)$
Optimization	Initial learning rate α_0	0.005	0.005	0.0002
	Decay coefficient κ	0.001	0.001	0.001
	Inner convergence τ	0.01	0.01	0.01
	Smoothing constant ϵ	10^{-4}	10^{-4}	10^{-4}
Algorithm-specific	Regularization λ	10^{-3}	10^{-3}	10^{-3}
	Exploration coefficient c	1.0	2.0	2.0
Training	Episodes	40,000	10,000	10,000
	Steps per episode	100	100	50
	Discount factor γ	0.99	0.99	0.99

4.2 Classic Control Environments

Tensor-based methods outperform matrix-based and neural baselines under matched parameter budgets. In Figure 2, LoRa-VI learns more slowly because CUR decomposition incurs higher parameter costs than CP factorization: CUR stores K anchor rows and columns, requiring $O(K(|\mathcal{S}| + |\mathcal{A}| - K))$ parameters. To match the budget, LoRa-VI uses only 3 buckets per state dimension in CartPole versus 10-20 for TEQL/TLR, which increases approximation bias.

Neural baselines do not merely exhibit slower learning but suffer from representational collapse under these extreme budgets. As the state-space expands, the fixed-capacity MLP fails to resolve the value landscape, whereas the tensor structure maintains a coherent global approximation by leveraging its intrinsic inductive bias rather than raw parameter

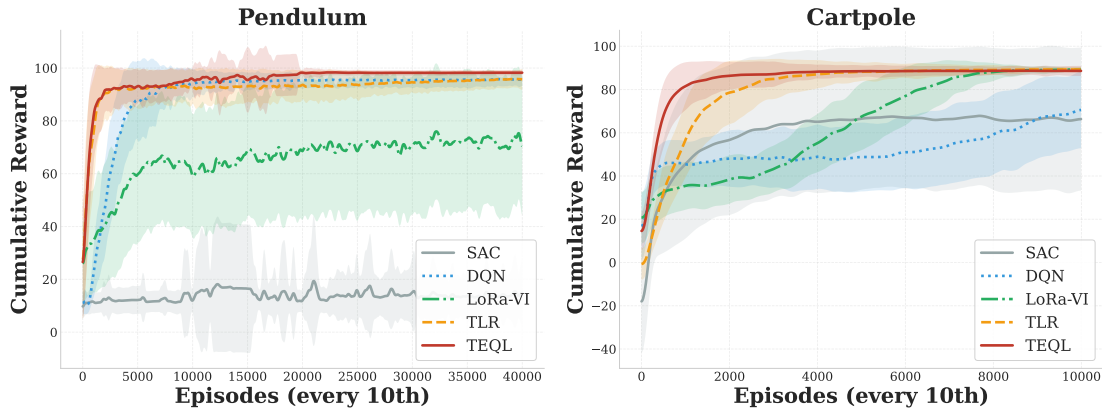


Figure 2: Learning curves on Pendulum (left) and CartPole (right). CP tensor methods (TEQL, TLR) outperform matrix-based (LoRa-VI) and neural baselines (DQN, SAC) under matched parameter budgets. The TEQL-TLR gap widens from Pendulum to CartPole as EUGE’s benefit increases with dimensionality. Shaded regions show mean \pm standard deviation over 100 runs.

count.

The advantage of TEQL over TLR scales with dimensionality. In Pendulum, the small state-action space allows uniform exploration to achieve reasonable coverage. In CartPole, the performance gap widens as undirected exploration becomes costly.

4.3 High-Dimensional Setting

The Highway environment simulates autonomous driving where an ego vehicle navigates multi-lane traffic. The nine-dimensional state space and safety-critical nature of the task make it a challenging testbed for evaluating scalability beyond the low-dimensional control tasks above.

As shown in Figure 3, TEQL reaches high performance around episode 5,000, approximately 2,000 episodes before TLR. DQN and SAC exhibit persistent instability, failing to retain high-reward policies once discovered. This stability gap in Highway underscores

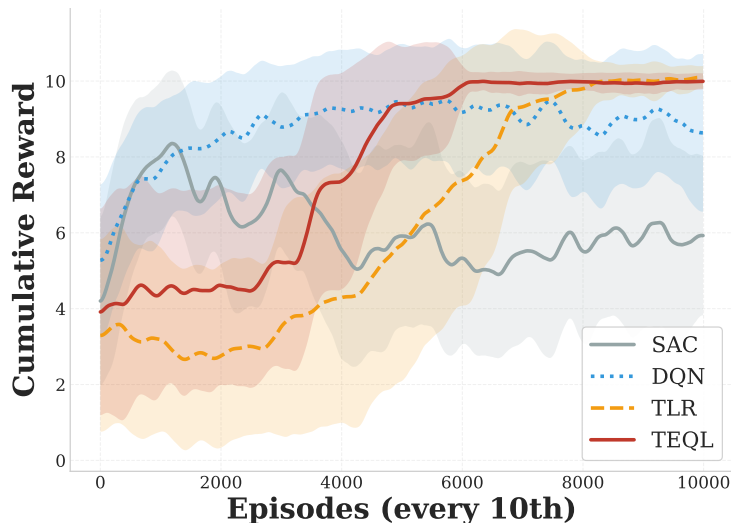


Figure 3: TEQL reaches high performance around episode 5,000, approximately 2,000 episodes before TLR. DQN oscillates; SAC regresses after initial progress. Highway: $D_S=9$, $D_A=1$.

the coupling effect detailed in Section 4.4: in high-dimensional manifolds, local updates in CP factors have global footprints, making frequency-aware regularization a prerequisite for structural integrity. LoRa-VI is excluded because CUR requires $O(|S|)$ parameters; additionally, narrow trajectory coverage makes leverage score estimation unreliable.

4.4 Ablation Study: Effect of Regularization Parameter λ

This section isolates the effect of frequency-aware regularization by comparing TLR, TEQL with $\lambda = 0$, and TEQL with $\lambda > 0$. All variants share identical CP structure, tensor rank, and TD update rules; only the regularization coefficient differs. Figure 4 shows learning curves, Figure 5 reports the distribution of cumulative rewards for last 2000 episodes.

The instability observed when $\lambda = 0$ reveals a structural vulnerability unique to CP factorization: because parameters in factor matrices are shared across the entire state-action fiber, updates in under-sampled regions propagate globally. This parameter sharing means that without regularization, overestimation at rarely visited pairs can corrupt Q-values

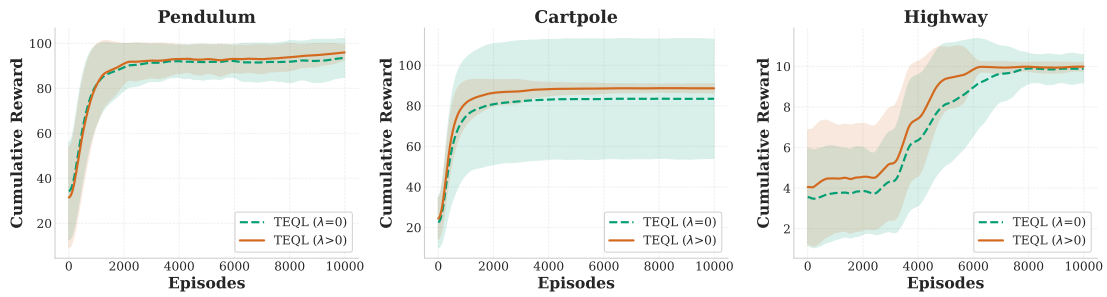


Figure 4: Learning curves for TEQL with $\lambda = 0$ and $\lambda > 0$. Setting $\lambda > 0$ reduces variance and achieves faster convergence across all environments.

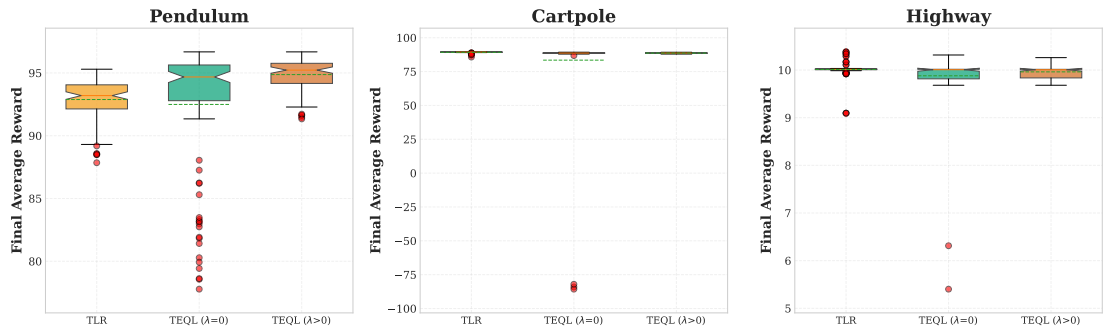


Figure 5: Distribution of final average rewards (last 200 episodes) over 100 runs. Setting $\lambda > 0$ substantially reduces standard deviation compared to $\lambda = 0$: from 5.24 to 1.30 on Pendulum, from 29.44 to 0.28 on CartPole, and from 0.59 to 0.12 on Highway.

throughout the tensor. The introduction of $\lambda > 0$ provides frequency-aware damping that specifically counteracts this effect: at sparsely visited pairs where overestimation risk is highest, the regularization coefficient $1/(\mathcal{N}_{t-1} + \epsilon)$ is large, resisting rapid value changes. As shown in Figure 5, the variance reduction scales with dimensionality: higher-dimensional environments exhibit sparser visitation patterns, making frequency-aware stabilization increasingly critical.

4.5 Sensitivity to Discretization Granularity

Performance gains in TEQL are tied to a realizability threshold where discretization resolution matches the requirements of the low-rank model class. Figure 6 reveals that under very

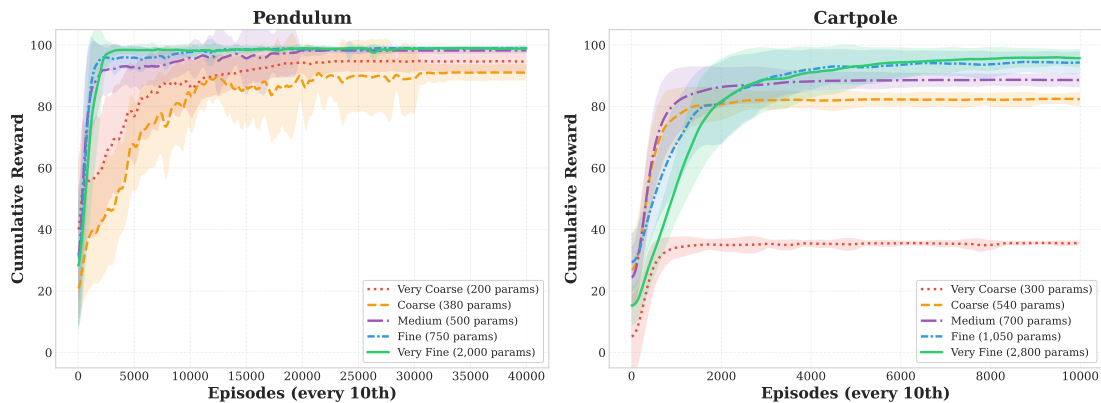


Figure 6: Coarse discretization limits final performance due to approximation bias; fine discretization allows near-optimal convergence. TEQL remains stable across all resolutions. Parameter counts: CartPole 300 to 2,800; Pendulum 200 to 2,000.

coarse discretization, TEQL converges reliably but to a suboptimal level. This plateau reflects the approximation bias B_R described in Theorem 1. Coarse binning collapses distinct dynamics into shared indices and produces a Q-function that lies outside the rank- R model class regardless of sample size. In this regime, the error is dominated by representation bias rather than by stochastic noise.

As resolution increases, performance improves before saturating at near-optimal levels. This transition marks the regime where the structural low-rank assumption becomes approximately satisfied and the convergence guarantees of TEQL become meaningful. Figure 7 compares TEQL and TLR under matched discretization across four granularity levels. At coarse granularity, both methods converge to similar suboptimal solutions because both are limited by B_R .

5 Conclusion

This work presents TEQL, a framework that uses low-rank tensor structure for sample-efficient reinforcement learning in high-dimensional discrete spaces. The core idea is that

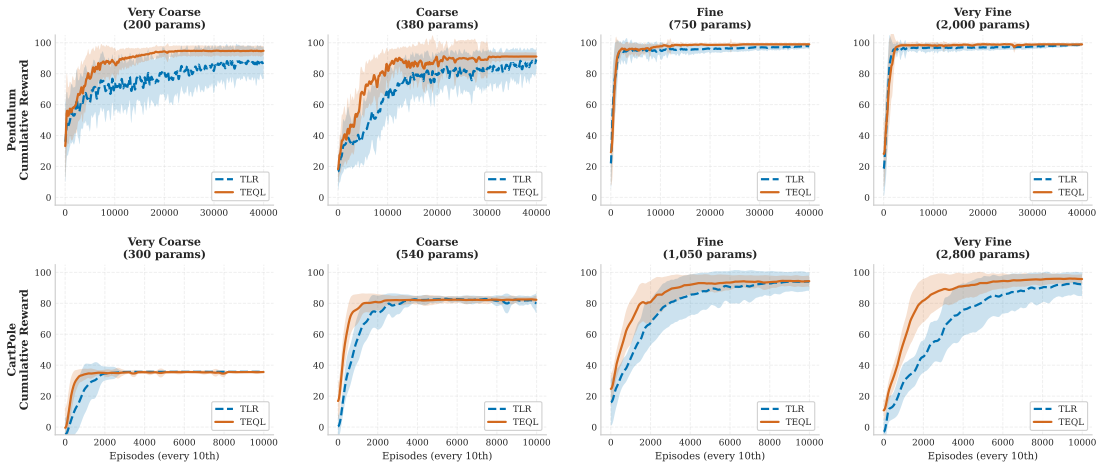


Figure 7: TLR vs TEQL under matched discretization. At coarse granularity, both methods are limited by approximation error B_R . At fine granularity, TEQL exhibits faster convergence and lower variance.

low-rank structure in value functions reflects the underlying problem: in many control tasks, state and action variables interact through a limited number of latent factors. This separability serves as a structured inductive bias for learning.

The major contribution of this work lies in reinforcement learning, where TEQL addresses an understudied area: efficient exploration in high-dimensional discrete state-action spaces where data collection is expensive. TEQL leverages tensor decomposition techniques and the EUGE mechanism to improve sample efficiency, which is useful in data-scarce scenarios such as clinical treatment optimization and inventory management. Existing tensor-based Q-learning methods (Rozada et al., 2024) rely on standard ϵ -greedy strategies without exploiting structural uncertainty, while continuous methods such as SAC are not designed for problems with a natural discrete structure. EUGE uses tensor reconstruction error as a low-cost measure of estimation uncertainty, and frequency-aware regularization addresses a vulnerability specific to CP-factored value functions: because factor entries are shared along entire state-action fibers, overestimation at a poorly visited pair can propagate globally through the shared parameters. From the tensor analysis perspective, this work

provides insights into how tensor decomposition can facilitate reinforcement learning based decision making. The Q-learning problem can be viewed as a tensor estimation problem in a sequential sampling scenario, and the EUGE exploration strategy demonstrates how uncertainty-driven sampling can be leveraged for more efficient tensor completion compared to uniform or random observation patterns.

TEQL is a sample-efficient learning strategy compared to neural network based approaches, and is particularly useful when sampling is expensive or data is scarce in discrete state-action domains. The CP representation achieves a reduction from exponential to linear in the number of dimensions, and provides an interpretable mode-wise factorization. However, since this method is based on the assumption of a low-rank tensor with the rank specified in advance, it is not applicable to problems where the value function does not admit a good low-rank approximation, for example when interactions across dimensions are highly entangled. For naturally continuous cases, as shown in the experiments, the performance improves as the discretization granularity increases, which indicates that for continuous state-action spaces this method might not be the most suitable. The performance of TEQL in such settings is not as strong as methods such as SAC that are designed for continuous cases. However, this does not diminish the contribution of TEQL in discrete action domains where data collection is expensive. The tensor rank R and discretization levels (d_1, \dots, d_N) are fixed before training; adaptive rank selection or resolution refinement during learning would improve flexibility but is not addressed in this work.

Future research will focus on extending this framework to continuous state and action spaces, where the discrete factor matrices would be replaced by continuous factor functions to eliminate discretization-induced approximation error. This combination of structured decomposition and continuous modeling provides a scalable direction for solving large-scale industrial control and resource optimization problems.

6 Data availability statement

The data that support the findings of this study were generated through simulation using standard benchmark environments. The source code implementing the proposed TEQL algorithm, together with scripts for reproducing the experiments and analysis, is openly available in a public repository at <https://github.com/Anonymous2025-cmd/teql-anon>.

References

- Agarwal, A., Kakade, S., Krishnamurthy, A., and Sun, W. (2020). FLAMBE: Structural complexity and representation learning of low rank MDPs. In *Advances in Neural Information Processing Systems*, volume 33, pages 20095–20107. Curran Associates, Inc.
- Auer, P., Cesa-Bianchi, N., and Fischer, P. (2002). Finite-time analysis of the multiarmed bandit problem. *Machine Learning*, 47(2-3):235–256.
- Bellman, R. (1957). *Dynamic Programming*. Princeton University Press.
- Bertsekas, D. P. and Tsitsiklis, J. N. (1996). *Neuro-Dynamic Programming*. Athena Scientific.
- Bradtke, S. J. and Barto, A. G. (1996). Linear least-squares algorithms for temporal difference learning. *Machine Learning*, 22(1-3):33–57.
- Christodoulou, P. (2019). Soft actor-critic for discrete action settings. *arXiv preprint arXiv:1910.07207*.
- Dadashi, R., Taiga, A. A., Roux, N. L., Schuurmans, D., and Bellemare, M. G. (2019). The value function polytope in reinforcement learning. In *International Conference on Machine Learning*, pages 1486–1495. PMLR.

- De Jonge, B. and Scarf, P. A. (2020). A review on maintenance optimization. *European Journal of Operational Research*, 285(3):805–824.
- Gheshlaghi Azar, M., Munos, R., and Kappen, H. J. (2013). Minimax pac bounds on the sample complexity of reinforcement learning with a generative model. In *International Conference on Machine Learning*, pages 72–80. PMLR.
- Gijsbrechts, J., Boute, R. N., Van Mieghem, J. A., and Zhang, D. J. (2022). Can deep reinforcement learning improve inventory management? Performance on dual sourcing, lost sales, and multi-echelon problems. *Manufacturing & Service Operations Management*, 24(3):1349–1368.
- Jaksch, T., Ortner, R., and Auer, P. (2010). Near-optimal regret bounds for reinforcement learning. *Journal of Machine Learning Research*, 11:1563–1600.
- Jiang, N., Krishnamurthy, A., Agarwal, A., Langford, J., and Schapire, R. E. (2017). Contextual decision processes with low Bellman rank are PAC-learnable. In *Proceedings of the 34th International Conference on Machine Learning*, volume 70 of *Proceedings of Machine Learning Research*, pages 1704–1713. PMLR.
- Komorowski, M., Celi, L. A., Badawi, O., Gordon, A. C., and Faisal, A. A. (2018). The artificial intelligence clinician learns optimal treatment strategies for sepsis in intensive care. *Nature Medicine*, 24(11):1716–1720.
- Liu, N., Liu, Y., Logan, B., Xu, Z., Tang, J., and Wang, Y. (2019). Learning the dynamic treatment regimes from medical registry data through deep q-network. *Scientific Reports*, 9(1):1–10.
- Mnih, V., Kavukcuoglu, K., Silver, D., Rusu, A. A., Veness, J., Bellemare, M. G., Graves, A., Riedmiller, M., Fidjeland, A. K., Ostrovski, G., et al. (2015). Human-level control through deep reinforcement learning. *Nature*, 518(7540):529–533.

- Modi, A., Chen, J., Krishnamurthy, A., Jiang, N., and Agarwal, A. (2024). Model-free representation learning and exploration in low-rank MDPs. *Journal of Machine Learning Research*, 25(6):1–76.
- Powell, W. B. (2007). *Approximate Dynamic Programming: Solving the Curses of Dimensionality*. Wiley.
- Puterman, M. L. (1994). *Markov Decision Processes: Discrete Stochastic Dynamic Programming*. Wiley.
- Rozada, S., Paternain, S., and Marques, A. G. (2024). Tensor and matrix low-rank value-function approximation in reinforcement learning. *IEEE Transactions on Signal Processing*, 72:1634–1649.
- Sam, Y., Maillard, O.-A., and Munos, R. (2023). Overcoming the curse of dimensionality in reinforcement learning through approximate factorization. *Advances in Neural Information Processing Systems*, 36.
- Shah, D., Song, D., Xu, Z., and Yang, Y. (2020). Sample efficient reinforcement learning via low-rank matrix estimation. arXiv preprint arXiv:2006.01527.
- Stojanovic, S., Jedra, Y., and Proutiere, A. (2024a). Model-free low-rank reinforcement learning via leveraged entry-wise matrix estimation. In *Advances in Neural Information Processing Systems*, volume 37, pages 30886–30924.
- Stojanovic, S., Jedra, Y., and Proutiere, A. (2024b). Model-free low-rank reinforcement learning via leveraged entry-wise matrix estimation. In *Advances in Neural Information Processing Systems*.
- Sutton, R. S. and Barto, A. G. (2018). *Reinforcement Learning: An Introduction*. MIT Press, 2 edition.

- Szepesvari, C. (2010). *Algorithms for Reinforcement Learning*, volume 4.
- Thrun, S. and Schwartz, A. (1993). Issues in using function approximation for reinforcement learning. In *Proceedings of the 1993 Connectionist Models Summer School*, pages 255–263, Hillsdale, NJ. Lawrence Erlbaum Associates.
- Tsai, K.-C., Zhuang, Z., Lent, R., Wang, J., Qi, Q., Wang, L.-C., and Han, Z. (2021). Tensor-based reinforcement learning for network routing. *IEEE Journal of Selected Topics in Signal Processing*, 15(3):640–653.
- Uehara, M., Zhang, X., and Sun, W. (2022). Representation learning for online and offline RL in low-rank MDPs. In *International Conference on Learning Representations*.
- Van Hasselt, H., Guez, A., and Silver, D. (2016). Deep reinforcement learning with double q-learning. In *Proceedings of the AAAI Conference on Artificial Intelligence*, pages 2094–2100.
- Watkins, C. J. C. H. and Dayan, P. (1992). Q-learning. *Machine Learning*, 8(3-4):279–292.
- Wu, C. F. J. and Hamada, M. S. (2011). *Experiments: Planning, Analysis, and Optimization*. John Wiley & Sons, 2 edition.
- Yang, Y., Zhang, G., Xu, Z.-W., and Katabi, D. (2020). Harnessing structures for value-based planning and reinforcement learning. In *International Conference on Learning Representations*.

7 Disclosure statement

The authors have no conflicts of interest to declare.

A Mathematical Proof

This section provides detailed proofs of the theoretical results stated in Section 3.4. For each result, we first restate the claim in precise mathematical form, then provide a complete proof with all intermediate steps explicitly shown.

Throughout, we use the notation established in the main text: \hat{Q}_t denotes the TEQL iterate at time t , q^* is the optimal Q-function, \mathcal{T} is the Bellman optimality operator, $V_{\max} = R_{\max}/(1 - \gamma)$ is the maximal value magnitude, $\mathcal{N}_{t-1}(s, a)$ is the visit count of pair (s, a) up to time $t - 1$, $\Delta Q_{t-1}(s, a)$ is the decomposition error defined in (8), and $\gamma \in (0, 1)$ is the discount factor.

By Assumption 1, the optimal Q-function q^* admits a rank- R CP approximation with error at most B_R . We further assume that this approximability extends to Bellman images of bounded low-rank tensors: for any rank- R tensor \mathcal{Q} with $\|\mathcal{Q}\|_{\infty} \leq V_{\max}$, the Bellman image $\mathcal{T}(\mathcal{Q})$ also admits a rank- R approximation with error at most B_R . This property, known as approximate Bellman closure, holds when the MDP transition dynamics exhibit low-rank or approximately low-rank structure.

A.1 Proof of Theorem 1

We first restate Theorem 1 in precise mathematical form.

Theorem 1 [Restatement] Under Assumptions 1 and 2, let ε_t denote the expected magnitude of the stochastic error at iteration t arising from using the single-sample TD target (6) instead of the full Bellman expectation. Then the TEQL iterates satisfy, for all $t \geq 1$,

$$\mathbb{E}[\|\hat{Q}_t - q^*\|_{\infty}] \leq \gamma^t \|\hat{Q}_0 - q^*\|_{\infty} + \frac{B_R}{1 - \gamma} + \sum_{k=0}^{t-1} \gamma^k \varepsilon_{t-1-k}. \quad (\text{A.1})$$

In the limit,

$$\limsup_{t \rightarrow \infty} \mathbb{E}[\|\hat{Q}_t - q^*\|_{\infty}] \leq \frac{B_R + \bar{\varepsilon}}{1 - \gamma}, \quad (\text{A.2})$$

where $\bar{\varepsilon} = \limsup_{t \rightarrow \infty} \varepsilon_t$.

The bound (A.1) decomposes the error into three terms: the initial error (decaying geometrically at rate γ), the approximation bias $B_R/(1 - \gamma)$ from Assumption 1, and the accumulated stochastic errors from single-sample TD updates. The asymptotic bound (A.2) shows that TEQL converges to a neighborhood of q^* with radius controlled by B_R and the noise level.

Proof. The proof proceeds in four steps. We first verify that Assumption 2 ensures the iterates remain in a domain where the Bellman closure property applies. We then decompose the approximation error using the structure of the Bellman operator, establish the contraction property, and expand the resulting recursion.

Step 1: Iterates Remain in the Bounded Domain.

By Assumption 2, $\|\hat{Q}_t\|_\infty \leq V_{\max}$ for all $t \geq 0$. This assumption can be enforced in practice by projecting or clipping the factor matrices $F_n^{(t)}$ after each update.

This boundedness condition ensures that the approximate Bellman closure property (stated at the beginning of this appendix) applies at every iteration. Specifically, since $\|\hat{Q}_{t-1}\|_\infty \leq V_{\max}$, the Bellman image $\mathcal{T}(\hat{Q}_{t-1})$ admits a rank- R approximation with error at most B_R . This property will be used in Step 3 to bound the projection error.

Step 2: Error Decomposition via Bellman Structure.

The Bellman optimality operator \mathcal{T} maps any Q-function Q to a new Q-function defined by

$$\mathcal{T}(Q)(s, a) = \mathbb{E}[r + \gamma \max_{a'} Q(s', a') \mid s, a], \quad (12)$$

where the expectation is taken over the distribution of rewards r and next states s' given the current state-action pair (s, a) , as determined by the MDP transition kernel \mathcal{P} and

reward function \mathcal{R} .

A fundamental property of the Bellman optimality operator is that the optimal Q-function q^* is its unique fixed point: $\mathcal{T}(q^*) = q^*$. This follows from the Bellman optimality equation, which states that for all (s, a) ,

$$q^*(s, a) = \mathbb{E}[r + \gamma \max_{a'} q^*(s', a') \mid s, a]. \quad (13)$$

The TEQL update can be modeled abstractly as follows. At each iteration t , the algorithm performs two operations: (i) it approximates the Bellman image $\mathcal{T}(\hat{Q}_{t-1})$ using a rank- R tensor via block coordinate descent, and (ii) it uses a single sampled transition (s_t, a_t, r_t, s_{t+1}) instead of the full expectation in the Bellman operator. We model this abstractly as

$$\hat{Q}_t = \Pi_R(\mathcal{T}(\hat{Q}_{t-1})) + \zeta_t, \quad (14)$$

where Π_R denotes a rank- R approximation operator, and ζ_t captures the stochastic error from using the single-sample TD target (6) instead of the full Bellman expectation.

The operator Π_R represents the outcome of the block coordinate descent procedure in Algorithm 1. By the approximate Bellman closure property established in Step 1, we have

$$\|\Pi_R(\mathcal{T}(Q)) - \mathcal{T}(Q)\|_\infty \leq B_R \quad (15)$$

for any Q with $\|Q\|_\infty \leq V_{\max}$.

We now decompose the error $\hat{Q}_t - q^*$. Starting from the abstract update (14), we subtract q^* from both sides:

$$\hat{Q}_t - q^* = \Pi_R(\mathcal{T}(\hat{Q}_{t-1})) + \zeta_t - q^*. \quad (16)$$

To reveal the structure of this error, we add and subtract intermediate terms. First, we add and subtract $\mathcal{T}(\hat{Q}_{t-1})$:

$$\hat{Q}_t - q^* = \Pi_R(\mathcal{T}(\hat{Q}_{t-1})) - \mathcal{T}(\hat{Q}_{t-1}) + \mathcal{T}(\hat{Q}_{t-1}) + \zeta_t - q^*. \quad (17)$$

Next, we add and subtract $\mathcal{T}(q^*)$:

$$\hat{Q}_t - q^* = \Pi_R(\mathcal{T}(\hat{Q}_{t-1})) - \mathcal{T}(\hat{Q}_{t-1}) + \mathcal{T}(\hat{Q}_{t-1}) - \mathcal{T}(q^*) + \mathcal{T}(q^*) + \zeta_t - q^*. \quad (18)$$

Using the fixed point property $\mathcal{T}(q^*) = q^*$, the terms $\mathcal{T}(q^*) - q^*$ cancel:

$$\hat{Q}_t - q^* = \underbrace{\Pi_R(\mathcal{T}(\hat{Q}_{t-1})) - \mathcal{T}(\hat{Q}_{t-1})}_{\text{projection error}} + \underbrace{\mathcal{T}(\hat{Q}_{t-1}) - \mathcal{T}(q^*)}_{\text{Bellman contraction term}} + \underbrace{\zeta_t}_{\text{stochastic error}}. \quad (19)$$

This decomposition identifies three sources of error: (i) The projection error arises from approximating the Bellman image by a rank- R tensor; (ii) The Bellman contraction term propagates the previous iteration's error through the Bellman operator. (iii) The stochastic error arises from using a single sampled transition instead of the full expectation.

Step 3: Contraction Property and One-Step Bound.

We now establish that the Bellman operator \mathcal{T} is a γ -contraction in the supremum norm. This is a classical result in dynamic programming, but we provide the full proof for completeness.

Let \mathcal{Q}_1 and \mathcal{Q}_2 be any two Q-functions. We want to show that

$$\|\mathcal{T}(\mathcal{Q}_1) - \mathcal{T}(\mathcal{Q}_2)\|_\infty \leq \gamma \|\mathcal{Q}_1 - \mathcal{Q}_2\|_\infty. \quad (20)$$

Fix any state-action pair (s, a) . By definition of the Bellman operator,

$$\begin{aligned} \mathcal{T}(\mathcal{Q}_1)(s, a) - \mathcal{T}(\mathcal{Q}_2)(s, a) &= \mathbb{E}[r + \gamma \max_{a'} \mathcal{Q}_1(s', a') \mid s, a] - \mathbb{E}[r + \gamma \max_{a'} \mathcal{Q}_2(s', a') \mid s, a]. \end{aligned} \quad (21)$$

Since the reward r is determined by the current state-action pair (s, a) and does not depend on the Q-function, the r terms cancel:

$$\begin{aligned} \mathcal{T}(\mathcal{Q}_1)(s, a) - \mathcal{T}(\mathcal{Q}_2)(s, a) &= \gamma \mathbb{E}[\max_{a'} \mathcal{Q}_1(s', a') \mid s, a] - \gamma \mathbb{E}[\max_{a'} \mathcal{Q}_2(s', a') \mid s, a] \\ &= \gamma \mathbb{E}[\max_{a'} \mathcal{Q}_1(s', a') - \max_{a'} \mathcal{Q}_2(s', a') \mid s, a], \end{aligned} \quad (22)$$

where we used the linearity of expectation in the last step.

Taking absolute values on both sides:

$$|\mathcal{T}(\mathcal{Q}_1)(s, a) - \mathcal{T}(\mathcal{Q}_2)(s, a)| = \gamma |\mathbb{E}[\max_{a'} \mathcal{Q}_1(s', a') - \max_{a'} \mathcal{Q}_2(s', a') \mid s, a]|. \quad (23)$$

By Jensen's inequality (or equivalently, the triangle inequality for integrals), the absolute value of an expectation is bounded by the expectation of the absolute value:

$$|\mathbb{E}[X]| \leq \mathbb{E}[|X|] \quad (24)$$

for any random variable X . Applying this:

$$|\mathcal{T}(\mathcal{Q}_1)(s, a) - \mathcal{T}(\mathcal{Q}_2)(s, a)| \leq \gamma \mathbb{E}[|\max_{a'} \mathcal{Q}_1(s', a') - \max_{a'} \mathcal{Q}_2(s', a')| \mid s, a]. \quad (25)$$

We now bound the term $|\max_{a'} \mathcal{Q}_1(s', a') - \max_{a'} \mathcal{Q}_2(s', a')|$ inside the expectation. We claim that for any two vectors $x = (x_1, \dots, x_m)$ and $y = (y_1, \dots, y_m)$,

$$|\max_i x_i - \max_i y_i| \leq \max_i |x_i - y_i|. \quad (26)$$

To prove (26), we consider two cases.

Case 1: Suppose $\max_i x_i \geq \max_i y_i$. Let $j = \arg \max_i x_i$, so $x_j = \max_i x_i$. Then:

$$\max_i x_i - \max_i y_i = x_j - \max_i y_i \quad (27)$$

$$\leq x_j - y_j \quad (\text{since } \max_i y_i \geq y_j) \quad (28)$$

$$\leq |x_j - y_j| \quad (29)$$

$$\leq \max_i |x_i - y_i|. \quad (30)$$

Since $\max_i x_i - \max_i y_i \geq 0$ in this case, we have $|\max_i x_i - \max_i y_i| = \max_i x_i - \max_i y_i \leq \max_i |x_i - y_i|$.

Case 2: Suppose $\max_i x_i < \max_i y_i$. By symmetry (swapping the roles of x and y in Case 1), we have $\max_i y_i - \max_i x_i \leq \max_i |y_i - x_i| = \max_i |x_i - y_i|$. Since $\max_i x_i - \max_i y_i < 0$ in this case, we have $|\max_i x_i - \max_i y_i| = \max_i y_i - \max_i x_i \leq \max_i |x_i - y_i|$.

In both cases, (26) holds.

Applying (26) to (25) with $x_{a'} = \mathcal{Q}_1(s', a')$ and $y_{a'} = \mathcal{Q}_2(s', a')$:

$$|\mathcal{T}(\mathcal{Q}_1)(s, a) - \mathcal{T}(\mathcal{Q}_2)(s, a)| \leq \gamma \mathbb{E}[\max_{a'} |\mathcal{Q}_1(s', a') - \mathcal{Q}_2(s', a')| | s, a]. \quad (31)$$

By definition of the supremum norm, for any s' :

$$\max_{a'} |\mathcal{Q}_1(s', a') - \mathcal{Q}_2(s', a')| \leq \sup_{s'', a''} |\mathcal{Q}_1(s'', a'') - \mathcal{Q}_2(s'', a'')| = \|\mathcal{Q}_1 - \mathcal{Q}_2\|_\infty. \quad (32)$$

Since $\|\mathcal{Q}_1 - \mathcal{Q}_2\|_\infty$ is a constant (independent of s'), the expectation of a constant equals the constant:

$$\mathbb{E}[\|\mathcal{Q}_1 - \mathcal{Q}_2\|_\infty | s, a] = \|\mathcal{Q}_1 - \mathcal{Q}_2\|_\infty. \quad (33)$$

Substituting into (31):

$$|\mathcal{T}(\mathcal{Q}_1)(s, a) - \mathcal{T}(\mathcal{Q}_2)(s, a)| \leq \gamma \|\mathcal{Q}_1 - \mathcal{Q}_2\|_\infty. \quad (34)$$

The inequality (34) holds for every (s, a) . Taking the supremum over all (s, a) on the left-hand side:

$$\|\mathcal{T}(\mathcal{Q}_1) - \mathcal{T}(\mathcal{Q}_2)\|_\infty = \sup_{s, a} |\mathcal{T}(\mathcal{Q}_1)(s, a) - \mathcal{T}(\mathcal{Q}_2)(s, a)| \leq \gamma \|\mathcal{Q}_1 - \mathcal{Q}_2\|_\infty. \quad (35)$$

This establishes that \mathcal{T} is a γ -contraction in the supremum norm.

We now use the error decomposition (19) and the contraction property (35) to derive a one-step bound.

Taking the supremum norm on both sides of (19):

$$\|\hat{Q}_t - q^*\|_\infty = \|[\Pi_R(\mathcal{T}(\hat{Q}_{t-1})) - \mathcal{T}(\hat{Q}_{t-1})] + [\mathcal{T}(\hat{Q}_{t-1}) - \mathcal{T}(q^*)] + \zeta_t\|_\infty. \quad (36)$$

Applying the triangle inequality for the supremum norm, which states that $\|f + g + h\|_\infty \leq \|f\|_\infty + \|g\|_\infty + \|h\|_\infty$:

$$\begin{aligned} \|\hat{Q}_t - q^*\|_\infty &\leq \|\Pi_R(\mathcal{T}(\hat{Q}_{t-1})) - \mathcal{T}(\hat{Q}_{t-1})\|_\infty \\ &\quad + \|\mathcal{T}(\hat{Q}_{t-1}) - \mathcal{T}(q^*)\|_\infty \\ &\quad + \|\zeta_t\|_\infty. \end{aligned} \quad (37)$$

We bound each of the three terms on the right-hand side.

Term 1 (projection error): By Step 1, we have $\|\hat{Q}_{t-1}\|_\infty \leq V_{\max}$. Therefore, the projection property (15) applies:

$$\|\Pi_R(\mathcal{T}(\hat{Q}_{t-1})) - \mathcal{T}(\hat{Q}_{t-1})\|_\infty \leq B_R. \quad (38)$$

Term 2 (Bellman contraction): Applying the contraction property (35) with $\mathcal{Q}_1 = \hat{Q}_{t-1}$ and $\mathcal{Q}_2 = q^*$:

$$\|\mathcal{T}(\hat{Q}_{t-1}) - \mathcal{T}(q^*)\|_\infty \leq \gamma \|\hat{Q}_{t-1} - q^*\|_\infty. \quad (39)$$

Term 3 (stochastic error): This term is $\|\zeta_t\|_\infty$, which we leave as is for now.

Substituting (38) and (39) into (37):

$$\|\hat{Q}_t - q^*\|_\infty \leq B_R + \gamma \|\hat{Q}_{t-1} - q^*\|_\infty + \|\zeta_t\|_\infty. \quad (40)$$

This is a deterministic inequality that holds for each realization of the stochastic process. To obtain a bound on the expected error, we take expectations on both sides.

Using the linearity of expectation:

$$\mathbb{E}[\|\hat{Q}_t - q^*\|_\infty] \leq \mathbb{E}[B_R] + \gamma \mathbb{E}[\|\hat{Q}_{t-1} - q^*\|_\infty] + \mathbb{E}[\|\zeta_t\|_\infty]. \quad (41)$$

Since B_R is a constant, $\mathbb{E}[B_R] = B_R$. Defining $\varepsilon_t := \mathbb{E}[\|\zeta_t\|_\infty]$ as in the theorem statement:

$$\mathbb{E}[\|\hat{Q}_t - q^*\|_\infty] \leq B_R + \gamma \mathbb{E}[\|\hat{Q}_{t-1} - q^*\|_\infty] + \varepsilon_t. \quad (42)$$

Step 4: Recursive Expansion and Limiting Behavior.

We now expand the recursion (42) to obtain explicit finite-time and asymptotic bounds.

Define $e_t := \mathbb{E}[\|\hat{Q}_t - q^*\|_\infty]$ for notational convenience. The recursion (42) becomes:

$$e_t \leq \gamma e_{t-1} + B_R + \varepsilon_t. \quad (43)$$

We expand this recursion by repeatedly substituting the bound for earlier terms.

Iteration 1: Starting from (43):

$$e_t \leq \gamma e_{t-1} + B_R + \varepsilon_t. \quad (44)$$

Iteration 2: Applying (43) to e_{t-1} , we have $e_{t-1} \leq \gamma e_{t-2} + B_R + \varepsilon_{t-1}$. Substituting:

$$e_t \leq \gamma(\gamma e_{t-2} + B_R + \varepsilon_{t-1}) + B_R + \varepsilon_t \quad (45)$$

$$= \gamma^2 e_{t-2} + \gamma B_R + B_R + \gamma \varepsilon_{t-1} + \varepsilon_t \quad (46)$$

$$= \gamma^2 e_{t-2} + (1 + \gamma)B_R + \gamma \varepsilon_{t-1} + \varepsilon_t. \quad (47)$$

Iteration 3: Applying (43) to e_{t-2} , we have $e_{t-2} \leq \gamma e_{t-3} + B_R + \varepsilon_{t-2}$. Substituting:

$$e_t \leq \gamma^2(\gamma e_{t-3} + B_R + \varepsilon_{t-2}) + (1 + \gamma)B_R + \gamma \varepsilon_{t-1} + \varepsilon_t \quad (48)$$

$$= \gamma^3 e_{t-3} + \gamma^2 B_R + (1 + \gamma)B_R + \gamma^2 \varepsilon_{t-2} + \gamma \varepsilon_{t-1} + \varepsilon_t \quad (49)$$

$$= \gamma^3 e_{t-3} + (1 + \gamma + \gamma^2)B_R + \gamma^2 \varepsilon_{t-2} + \gamma \varepsilon_{t-1} + \varepsilon_t. \quad (50)$$

General pattern: After k iterations of this expansion, we have:

$$e_t \leq \gamma^k e_{t-k} + B_R \sum_{j=0}^{k-1} \gamma^j + \sum_{j=0}^{k-1} \gamma^j \varepsilon_{t-1-j}. \quad (51)$$

We verify this pattern by induction. The base case $k = 1$ is (43). For the inductive step, assume (51) holds for some k . Applying (43) to e_{t-k} :

$$e_t \leq \gamma^k(\gamma e_{t-k-1} + B_R + \varepsilon_{t-k}) + B_R \sum_{j=0}^{k-1} \gamma^j + \sum_{j=0}^{k-1} \gamma^j \varepsilon_{t-1-j} \quad (52)$$

$$= \gamma^{k+1} e_{t-k-1} + \gamma^k B_R + B_R \sum_{j=0}^{k-1} \gamma^j + \gamma^k \varepsilon_{t-k} + \sum_{j=0}^{k-1} \gamma^j \varepsilon_{t-1-j} \quad (53)$$

$$= \gamma^{k+1} e_{t-k-1} + B_R \sum_{j=0}^k \gamma^j + \sum_{j=0}^k \gamma^j \varepsilon_{t-1-j}, \quad (54)$$

which is (51) with k replaced by $k + 1$.

Full expansion: Setting $k = t$ in (51), so that $e_{t-k} = e_0$:

$$e_t \leq \gamma^t e_0 + B_R \sum_{j=0}^{t-1} \gamma^j + \sum_{j=0}^{t-1} \gamma^j \varepsilon_{t-1-j}. \quad (55)$$

The initial error $e_0 = \mathbb{E}[\|\hat{Q}_0 - q^*\|_\infty] = \|\hat{Q}_0 - q^*\|_\infty$ is deterministic (given the initialization).

For the geometric sum, we use the standard formula. For $\gamma \neq 1$:

$$\sum_{j=0}^{t-1} \gamma^j = \frac{1 - \gamma^t}{1 - \gamma}. \quad (56)$$

Since $0 < \gamma < 1$, we have $0 < \gamma^t < 1$, so $1 - \gamma^t < 1$. Therefore:

$$\sum_{j=0}^{t-1} \gamma^j = \frac{1 - \gamma^t}{1 - \gamma} < \frac{1}{1 - \gamma}. \quad (57)$$

Substituting (57) into (55):

$$e_t \leq \gamma^t \|\hat{Q}_0 - q^*\|_\infty + \frac{B_R}{1 - \gamma} + \sum_{j=0}^{t-1} \gamma^j \varepsilon_{t-1-j}. \quad (58)$$

This establishes the finite-time bound (A.1).

Asymptotic bound: We now derive the limiting bound (A.2) by analyzing the behavior of each term in (58) as $t \rightarrow \infty$.

Term 1: Since $0 < \gamma < 1$, we have $\lim_{t \rightarrow \infty} \gamma^t = 0$. Therefore:

$$\lim_{t \rightarrow \infty} \gamma^t \|\hat{Q}_0 - q^*\|_\infty = 0. \quad (59)$$

Term 2: The term $\frac{B_R}{1-\gamma}$ is a constant, independent of t .

Term 3: We show that $\limsup_{t \rightarrow \infty} \sum_{j=0}^{t-1} \gamma^j \varepsilon_{t-1-j} \leq \frac{\bar{\varepsilon}}{1-\gamma}$, where $\bar{\varepsilon} = \limsup_{t \rightarrow \infty} \varepsilon_t$.

By the definition of \limsup , for any $\eta > 0$, there exists $t_\eta \geq 1$ such that $\varepsilon_t \leq \bar{\varepsilon} + \eta$ for all $t \geq t_\eta$.

We split the sum $\sum_{j=0}^{t-1} \gamma^j \varepsilon_{t-1-j}$ into two parts based on whether the index $t-1-j$ is at least t_η or not:

$$\sum_{j=0}^{t-1} \gamma^j \varepsilon_{t-1-j} = \underbrace{\sum_{j=0}^{t-t_\eta-1} \gamma^j \varepsilon_{t-1-j}}_{\text{Part A}} + \underbrace{\sum_{j=t-t_\eta}^{t-1} \gamma^j \varepsilon_{t-1-j}}_{\text{Part B}}. \quad (60)$$

Part A: For j in the range $0 \leq j \leq t-t_\eta-1$, the index $t-1-j$ ranges from $(t-1)-0 = t-1$ down to $(t-1)-(t-t_\eta-1) = t_\eta$. Since all these indices are at least t_η , we have $\varepsilon_{t-1-j} \leq \bar{\varepsilon} + \eta$ for each term. Therefore:

$$\sum_{j=0}^{t-t_\eta-1} \gamma^j \varepsilon_{t-1-j} \leq \sum_{j=0}^{t-t_\eta-1} \gamma^j (\bar{\varepsilon} + \eta) \quad (61)$$

$$= (\bar{\varepsilon} + \eta) \sum_{j=0}^{t-t_\eta-1} \gamma^j \quad (62)$$

$$\leq (\bar{\varepsilon} + \eta) \sum_{j=0}^{\infty} \gamma^j \quad (63)$$

$$= (\bar{\varepsilon} + \eta) \cdot \frac{1}{1-\gamma} \quad (64)$$

$$= \frac{\bar{\varepsilon} + \eta}{1-\gamma}. \quad (65)$$

Part B: For j in the range $t-t_\eta \leq j \leq t-1$, the index $t-1-j$ ranges from $(t-1)-(t-t_\eta) = t_\eta - 1$ down to $(t-1) - (t-1) = 0$. Let $M := \max_{0 \leq s \leq t_\eta-1} \varepsilon_s$, which is a finite constant

depending only on t_η (and hence only on η). Then:

$$\sum_{j=t-t_\eta}^{t-1} \gamma^j \varepsilon_{t-1-j} \leq \sum_{j=t-t_\eta}^{t-1} \gamma^j \cdot M \quad (66)$$

$$= M \sum_{j=t-t_\eta}^{t-1} \gamma^j. \quad (67)$$

To evaluate the sum $\sum_{j=t-t_\eta}^{t-1} \gamma^j$, we substitute $k = j - (t - t_\eta)$, so k ranges from 0 to $t_\eta - 1$:

$$\sum_{j=t-t_\eta}^{t-1} \gamma^j = \sum_{k=0}^{t_\eta-1} \gamma^{k+(t-t_\eta)} \quad (68)$$

$$= \gamma^{t-t_\eta} \sum_{k=0}^{t_\eta-1} \gamma^k \quad (69)$$

$$\leq \gamma^{t-t_\eta} \cdot \frac{1}{1-\gamma}. \quad (70)$$

Therefore:

$$\sum_{j=t-t_\eta}^{t-1} \gamma^j \varepsilon_{t-1-j} \leq M \cdot \gamma^{t-t_\eta} \cdot \frac{1}{1-\gamma} = \frac{M\gamma^{t-t_\eta}}{1-\gamma}. \quad (71)$$

Combining (65) and (71):

$$\sum_{j=0}^{t-1} \gamma^j \varepsilon_{t-1-j} \leq \frac{\bar{\varepsilon} + \eta}{1-\gamma} + \frac{M\gamma^{t-t_\eta}}{1-\gamma}. \quad (72)$$

Taking $t \rightarrow \infty$ while holding η (and hence t_η and M) fixed: since $0 < \gamma < 1$, we have

$\gamma^{t-t_\eta} \rightarrow 0$ as $t \rightarrow \infty$. Therefore:

$$\limsup_{t \rightarrow \infty} \sum_{j=0}^{t-1} \gamma^j \varepsilon_{t-1-j} \leq \frac{\bar{\varepsilon} + \eta}{1-\gamma} + 0 = \frac{\bar{\varepsilon} + \eta}{1-\gamma}. \quad (73)$$

Since this holds for all $\eta > 0$, taking $\eta \rightarrow 0$:

$$\limsup_{t \rightarrow \infty} \sum_{j=0}^{t-1} \gamma^j \varepsilon_{t-1-j} \leq \frac{\bar{\varepsilon}}{1-\gamma}. \quad (74)$$

Combining all three terms, we take the lim sup of (58):

$$\limsup_{t \rightarrow \infty} e_t \leq \limsup_{t \rightarrow \infty} \gamma^t \|\hat{Q}_0 - q^*\|_\infty + \frac{B_R}{1-\gamma} + \limsup_{t \rightarrow \infty} \sum_{j=0}^{t-1} \gamma^j \varepsilon_{t-1-j} \quad (75)$$

$$\leq 0 + \frac{B_R}{1-\gamma} + \frac{\bar{\varepsilon}}{1-\gamma} \quad (76)$$

$$= \frac{B_R + \bar{\varepsilon}}{1-\gamma}. \quad (77)$$

This establishes the asymptotic bound (A.2) and completes the proof of Theorem 1. \square

A.2 Proof of Proposition 1

We first restate Proposition 1 in precise mathematical form.

Proposition 1[Restatement] Under Assumption 2, suppose the factor matrices $\{F_n^{(t)}\}_{n=1}^N$ satisfy $\|F_n^{(t)}\|_\infty \leq F_{\max}$ for all n and t (enforceable via projection). For a single block coordinate descent sweep with step size α_t , the decomposition error defined in (8) satisfies

$$\Delta \mathcal{Q}_t(s_t, a_t) \leq \alpha_t \cdot 2NR F_{\max}^{2(N-1)} V_{\max} + \alpha_t \cdot \frac{2\lambda N R F_{\max}^{2(N-1)} V_{\max}}{\mathcal{N}_{t-1}(s_t, a_t) + \epsilon}. \quad (\text{A.3})$$

The bound (A.3) shows that the decomposition error has two components: a baseline term proportional to α_t and a term that decreases as $1/(\mathcal{N}_{t-1}(s_t, a_t) + \epsilon)$ grows. This formalizes the claim that frequency regularization makes updates smaller on frequently visited pairs.

Proof. We derive the bound by computing the gradient of the TEQL objective with respect to the factor matrices and tracking how a single block coordinate descent sweep changes the Q-value at the sampled state-action pair. We upper bound one full BCD sweep by considering a gradient-type update per mode and applying the triangle inequality across modes.

Step 1: Setup and Loss Function.

Fix the sampled pair (s_t, a_t) with corresponding multi-index (i_1, \dots, i_N) in the tensor representation, where $N = D_S + D_A$ is the total number of state and action dimensions.

The TEQL per-sample loss function, as given in (7), is

$$L_{s_t, a_t} = \frac{1}{2} (q_t^{\text{target}}(s_t, a_t) - \hat{Q}_t(s_t, a_t))^2 - \lambda \frac{\hat{Q}_t(s_t, a_t)^2}{\mathcal{N}_{t-1}(s_t, a_t) + \epsilon}, \quad (78)$$

where:

- $q_t^{\text{target}}(s_t, a_t) = r_t + \gamma \max_{a'} \hat{Q}_{t-1}(s_{t+1}, a')$ is the TD target defined in (6), treated as a constant during the factor update;
- $\lambda > 0$ is the regularization parameter;
- $\epsilon > 0$ is a small constant to avoid division by zero;
- $\mathcal{N}_{t-1}(s_t, a_t)$ is the visit count of (s_t, a_t) before time t .

The first term is the squared TD error, which drives the Q-function toward the Bellman target. The second term is the frequency regularizer, which penalizes large Q-values at frequently visited state-action pairs by an amount inversely proportional to the visit count.

Step 2: CP Representation and Gradient Computation.

By the CP decomposition, the Q-value at (s_t, a_t) is

$$\hat{Q}_t(s_t, a_t) = \sum_{r=1}^R \prod_{n=1}^N F_n^{(t)}(i_n, r), \quad (79)$$

where $F_n^{(t)} \in \mathbb{R}^{d_n \times R}$ are the factor matrices at time t , and R is the CP rank.

Consider updating mode n while holding the other factor matrices $\{F_m^{(t)}\}_{m \neq n}$ fixed. We compute the partial derivative of $\hat{Q}_t(s_t, a_t)$ with respect to the factor entry $F_n^{(t)}(i_n, r)$.

From (79), only the r -th term in the sum depends on $F_n^{(t)}(i_n, r)$:

$$\frac{\partial}{\partial F_n^{(t)}(i_n, r)} \sum_{r'=1}^R \prod_{m=1}^N F_m^{(t)}(i_m, r') = \frac{\partial}{\partial F_n^{(t)}(i_n, r)} \prod_{m=1}^N F_m^{(t)}(i_m, r). \quad (80)$$

The product $\prod_{m=1}^N F_m^{(t)}(i_m, r)$ is linear in $F_n^{(t)}(i_n, r)$, so:

$$\frac{\partial}{\partial F_n^{(t)}(i_n, r)} \prod_{m=1}^N F_m^{(t)}(i_m, r) = \prod_{m \neq n} F_m^{(t)}(i_m, r). \quad (81)$$

Now we compute the gradient of the loss (78). The loss consists of two terms, and we differentiate each separately.

First term (squared TD error): Let $f(\hat{Q}) = \frac{1}{2}(q_t^{\text{target}} - \hat{Q})^2$. By the chain rule:

$$\frac{\partial f}{\partial F_n^{(t)}(i_n, r)} = \frac{\partial f}{\partial \hat{Q}_t} \cdot \frac{\partial \hat{Q}_t}{\partial F_n^{(t)}(i_n, r)}. \quad (82)$$

We have:

$$\frac{\partial f}{\partial \hat{Q}_t} = \frac{\partial}{\partial \hat{Q}_t} \left[\frac{1}{2}(q_t^{\text{target}} - \hat{Q}_t)^2 \right] = (q_t^{\text{target}} - \hat{Q}_t) \cdot (-1) = -(q_t^{\text{target}} - \hat{Q}_t(s_t, a_t)). \quad (83)$$

Combining with (81):

$$\frac{\partial}{\partial F_n^{(t)}(i_n, r)} \left[\frac{1}{2}(q_t^{\text{target}} - \hat{Q}_t)^2 \right] = -(q_t^{\text{target}} - \hat{Q}_t(s_t, a_t)) \prod_{m \neq n} F_m^{(t)}(i_m, r). \quad (84)$$

Second term (frequency regularizer): Let $g(\hat{Q}) = -\lambda \frac{\hat{Q}^2}{\mathcal{N}_{t-1}(s_t, a_t) + \epsilon}$. By the chain rule:

$$\frac{\partial g}{\partial F_n^{(t)}(i_n, r)} = \frac{\partial g}{\partial \hat{Q}_t} \cdot \frac{\partial \hat{Q}_t}{\partial F_n^{(t)}(i_n, r)}. \quad (85)$$

We have:

$$\frac{\partial g}{\partial \hat{Q}_t} = \frac{\partial}{\partial \hat{Q}_t} \left[-\lambda \frac{\hat{Q}_t^2}{\mathcal{N}_{t-1}(s_t, a_t) + \epsilon} \right] = -\lambda \cdot \frac{2\hat{Q}_t}{\mathcal{N}_{t-1}(s_t, a_t) + \epsilon} = -\frac{2\lambda \hat{Q}_t(s_t, a_t)}{\mathcal{N}_{t-1}(s_t, a_t) + \epsilon}. \quad (86)$$

Combining with (81):

$$\frac{\partial}{\partial F_n^{(t)}(i_n, r)} \left[-\lambda \frac{\hat{Q}_t^2}{\mathcal{N}_{t-1}(s_t, a_t) + \epsilon} \right] = -\frac{2\lambda \hat{Q}_t(s_t, a_t)}{\mathcal{N}_{t-1}(s_t, a_t) + \epsilon} \prod_{m \neq n} F_m^{(t)}(i_m, r). \quad (87)$$

Full gradient: Adding (84) and (87):

$$\begin{aligned}
\nabla_{F_n(i_n, r)} L_{s_t, a_t} &= -(q_t^{\text{target}} - \hat{Q}_t(s_t, a_t)) \prod_{m \neq n} F_m(i_m, r) - \frac{2\lambda \hat{Q}_t(s_t, a_t)}{\mathcal{N}_{t-1}(s_t, a_t) + \epsilon} \prod_{m \neq n} F_m(i_m, r) \\
&= \left[-(q_t^{\text{target}} - \hat{Q}_t(s_t, a_t)) - \frac{2\lambda \hat{Q}_t(s_t, a_t)}{\mathcal{N}_{t-1}(s_t, a_t) + \epsilon} \right] \prod_{m \neq n} F_m(i_m, r) \\
&= \left[(\hat{Q}_t(s_t, a_t) - q_t^{\text{target}}) - \frac{2\lambda \hat{Q}_t(s_t, a_t)}{\mathcal{N}_{t-1}(s_t, a_t) + \epsilon} \right] \prod_{m \neq n} F_m(i_m, r). \tag{88}
\end{aligned}$$

This matches the gradient formula (9) in the main text.

Step 3: Factor Update and Induced Change in Q-Value.

By the factor update rule (10), a gradient descent step with step size α_t updates the factor entry as:

$$F_n^{(t)}(i_n, r) \leftarrow F_n^{(t)}(i_n, r) - \alpha_t \nabla_{F_n(i_n, r)} L_{s_t, a_t}. \tag{89}$$

The change in the factor entry is:

$$\Delta F_n^{(t)}(i_n, r) := F_n^{(t), \text{new}}(i_n, r) - F_n^{(t), \text{old}}(i_n, r) = -\alpha_t \nabla_{F_n(i_n, r)} L_{s_t, a_t}. \tag{90}$$

Substituting the gradient (88):

$$\Delta F_n^{(t)}(i_n, r) = -\alpha_t \left[(\hat{Q}_t(s_t, a_t) - q_t^{\text{target}}) - \frac{2\lambda \hat{Q}_t(s_t, a_t)}{\mathcal{N}_{t-1}(s_t, a_t) + \epsilon} \right] \prod_{m \neq n} F_m(i_m, r). \tag{91}$$

The induced change in $\hat{Q}_t(s_t, a_t)$ from updating mode n (while holding other modes fixed) is computed as follows. By the CP representation (79):

$$\begin{aligned}
\Delta_n \hat{Q}_t(s_t, a_t) &:= \hat{Q}_t^{\text{new}}(s_t, a_t) - \hat{Q}_t^{\text{old}}(s_t, a_t) \\
&= \sum_{r=1}^R \left[\prod_{m=1}^N F_m^{\text{new}}(i_m, r) - \prod_{m=1}^N F_m^{\text{old}}(i_m, r) \right]. \tag{92}
\end{aligned}$$

Since only mode n is updated and all other modes remain fixed, we have $F_m^{\text{new}}(i_m, r) =$

$F_m^{\text{old}}(i_m, r)$ for $m \neq n$. Therefore:

$$\begin{aligned}
\prod_{m=1}^N F_m^{\text{new}}(i_m, r) - \prod_{m=1}^N F_m^{\text{old}}(i_m, r) &= F_n^{\text{new}}(i_n, r) \prod_{m \neq n} F_m(i_m, r) - F_n^{\text{old}}(i_n, r) \prod_{m \neq n} F_m(i_m, r) \\
&= [F_n^{\text{new}}(i_n, r) - F_n^{\text{old}}(i_n, r)] \prod_{m \neq n} F_m(i_m, r) \\
&= \Delta F_n^{(t)}(i_n, r) \cdot \prod_{m \neq n} F_m(i_m, r). \tag{93}
\end{aligned}$$

Summing over r :

$$\Delta_n \hat{Q}_t(s_t, a_t) = \sum_{r=1}^R \Delta F_n^{(t)}(i_n, r) \cdot \prod_{m \neq n} F_m(i_m, r). \tag{94}$$

Substituting (91) into (94):

$$\begin{aligned}
\Delta_n \hat{Q}_t(s_t, a_t) &= \sum_{r=1}^R \left\{ -\alpha_t \left[(\hat{Q}_t - q_t^{\text{target}}) - \frac{2\lambda \hat{Q}_t}{\mathcal{N}_{t-1} + \epsilon} \right] \prod_{m \neq n} F_m(i_m, r) \right\} \cdot \prod_{m \neq n} F_m(i_m, r) \\
&= -\alpha_t \left[(\hat{Q}_t - q_t^{\text{target}}) - \frac{2\lambda \hat{Q}_t}{\mathcal{N}_{t-1} + \epsilon} \right] \sum_{r=1}^R \left(\prod_{m \neq n} F_m(i_m, r) \right)^2, \tag{95}
\end{aligned}$$

where we abbreviated $\hat{Q}_t = \hat{Q}_t(s_t, a_t)$ and $\mathcal{N}_{t-1} = \mathcal{N}_{t-1}(s_t, a_t)$ for readability.

Taking absolute values:

$$|\Delta_n \hat{Q}_t(s_t, a_t)| = \alpha_t \left| (\hat{Q}_t - q_t^{\text{target}}) - \frac{2\lambda \hat{Q}_t}{\mathcal{N}_{t-1} + \epsilon} \right| \sum_{r=1}^R \left(\prod_{m \neq n} F_m(i_m, r) \right)^2. \tag{96}$$

Step 4: Bounding the Product of Factor Entries.

We now bound $\sum_{r=1}^R (\prod_{m \neq n} F_m(i_m, r))^2$.

By assumption, each factor entry satisfies $|F_m^{(t)}(i_m, r)| \leq F_{\max}$ for all m, r , and t . Therefore, for each r :

$$\left| \prod_{m \neq n} F_m(i_m, r) \right| = \prod_{m \neq n} |F_m(i_m, r)| \leq \prod_{m \neq n} F_{\max} = F_{\max}^{N-1}, \tag{97}$$

where the product is over $N - 1$ terms (all modes except mode n).

Squaring both sides:

$$\left(\prod_{m \neq n} F_m(i_m, r) \right)^2 \leq F_{\max}^{2(N-1)}. \quad (98)$$

Summing over $r = 1, \dots, R$:

$$\sum_{r=1}^R \left(\prod_{m \neq n} F_m(i_m, r) \right)^2 \leq \sum_{r=1}^R F_{\max}^{2(N-1)} = R \cdot F_{\max}^{2(N-1)}. \quad (99)$$

Step 5: Bounding the Bracket Term.

We now bound the term $\left| (\hat{Q}_t - q_t^{\text{target}}) - \frac{2\lambda\hat{Q}_t}{\mathcal{N}_{t-1} + \epsilon} \right|$ in (96).

By the triangle inequality, for any real numbers a and b :

$$|a - b| \leq |a| + |b|. \quad (100)$$

Applying this with $a = \hat{Q}_t - q_t^{\text{target}}$ and $b = \frac{2\lambda\hat{Q}_t}{\mathcal{N}_{t-1} + \epsilon}$:

$$\left| (\hat{Q}_t - q_t^{\text{target}}) - \frac{2\lambda\hat{Q}_t}{\mathcal{N}_{t-1} + \epsilon} \right| \leq |\hat{Q}_t - q_t^{\text{target}}| + \frac{2\lambda|\hat{Q}_t|}{\mathcal{N}_{t-1} + \epsilon}. \quad (101)$$

We bound each term on the right-hand side separately.

Bounding $|\hat{Q}_t(s_t, a_t)|$: By Assumption 2, $\|\hat{Q}_t\|_{\infty} \leq V_{\max}$, so:

$$|\hat{Q}_t(s_t, a_t)| \leq V_{\max}. \quad (102)$$

Bounding $|q_t^{\text{target}}(s_t, a_t)|$: By definition (6):

$$q_t^{\text{target}}(s_t, a_t) = r_t + \gamma \max_{a'} \hat{Q}_{t-1}(s_{t+1}, a'). \quad (103)$$

Taking absolute values and applying the triangle inequality:

$$\begin{aligned} |q_t^{\text{target}}(s_t, a_t)| &= |r_t + \gamma \max_{a'} \hat{Q}_{t-1}(s_{t+1}, a')| \\ &\leq |r_t| + \gamma |\max_{a'} \hat{Q}_{t-1}(s_{t+1}, a')|. \end{aligned} \quad (104)$$

By the bounded rewards assumption, $|r_t| \leq R_{\max}$. By Assumption 2, $|\max_{a'} \hat{Q}_{t-1}(s_{t+1}, a')| \leq \|\hat{Q}_{t-1}\|_{\infty} \leq V_{\max}$. Therefore:

$$|q_t^{\text{target}}(s_t, a_t)| \leq R_{\max} + \gamma V_{\max}. \quad (105)$$

Bounding $|\hat{Q}_t - q_t^{\text{target}}|$: Applying the triangle inequality:

$$\begin{aligned} |\hat{Q}_t(s_t, a_t) - q_t^{\text{target}}(s_t, a_t)| &\leq |\hat{Q}_t(s_t, a_t)| + |q_t^{\text{target}}(s_t, a_t)| \\ &\leq V_{\max} + (R_{\max} + \gamma V_{\max}) \\ &= V_{\max} + R_{\max} + \gamma V_{\max}. \end{aligned} \quad (106)$$

We simplify using the relationship $V_{\max} = R_{\max}/(1-\gamma)$, which implies $R_{\max} = (1-\gamma)V_{\max}$.

Substituting:

$$\begin{aligned} V_{\max} + R_{\max} + \gamma V_{\max} &= V_{\max} + (1-\gamma)V_{\max} + \gamma V_{\max} \\ &= V_{\max} + V_{\max} - \gamma V_{\max} + \gamma V_{\max} \\ &= 2V_{\max}. \end{aligned} \quad (107)$$

Therefore:

$$|\hat{Q}_t(s_t, a_t) - q_t^{\text{target}}(s_t, a_t)| \leq 2V_{\max}. \quad (108)$$

Substituting (102) and (108) into (101):

$$\left| (\hat{Q}_t - q_t^{\text{target}}) - \frac{2\lambda\hat{Q}_t}{\mathcal{N}_{t-1} + \epsilon} \right| \leq 2V_{\max} + \frac{2\lambda V_{\max}}{\mathcal{N}_{t-1}(s_t, a_t) + \epsilon}. \quad (109)$$

Step 6: Bounding the Change from Mode n .

Substituting (99) and (109) into (96):

$$\begin{aligned} |\Delta_n \hat{Q}_t(s_t, a_t)| &\leq \alpha_t \left(2V_{\max} + \frac{2\lambda V_{\max}}{\mathcal{N}_{t-1}(s_t, a_t) + \epsilon} \right) \cdot R \cdot F_{\max}^{2(N-1)} \\ &= \alpha_t \cdot R F_{\max}^{2(N-1)} \cdot 2V_{\max} + \alpha_t \cdot R F_{\max}^{2(N-1)} \cdot \frac{2\lambda V_{\max}}{\mathcal{N}_{t-1}(s_t, a_t) + \epsilon}. \end{aligned} \quad (110)$$

Step 7: Summing Over All Modes.

A full block coordinate descent sweep updates all N modes sequentially. Although the factor entries change as earlier modes are updated, the bound $|F_m(i_m, r)| \leq F_{\max}$ holds uniformly throughout the sweep (by the boundedness assumption or by enforcing projection after each mode update). Therefore, the bound (110) applies to each mode update.

The total change in $\hat{Q}_t(s_t, a_t)$ from the full sweep is:

$$\Delta Q_t(s_t, a_t) = |\hat{Q}_t(s_t, a_t) - \hat{Q}_{t-1}(s_t, a_t)|, \quad (111)$$

as defined in (8).

The change can be written as the sum of changes from each mode. By the triangle inequality:

$$\Delta Q_t(s_t, a_t) = \left| \sum_{n=1}^N \Delta_n \hat{Q}_t(s_t, a_t) \right| \leq \sum_{n=1}^N |\Delta_n \hat{Q}_t(s_t, a_t)|. \quad (112)$$

Substituting (110) for each mode:

$$\begin{aligned} \Delta Q_t(s_t, a_t) &\leq \sum_{n=1}^N \left[\alpha_t \cdot RF_{\max}^{2(N-1)} \cdot 2V_{\max} + \alpha_t \cdot RF_{\max}^{2(N-1)} \cdot \frac{2\lambda V_{\max}}{\mathcal{N}_{t-1}(s_t, a_t) + \epsilon} \right] \\ &= N \cdot \alpha_t \cdot RF_{\max}^{2(N-1)} \cdot 2V_{\max} + N \cdot \alpha_t \cdot RF_{\max}^{2(N-1)} \cdot \frac{2\lambda V_{\max}}{\mathcal{N}_{t-1}(s_t, a_t) + \epsilon} \\ &= \alpha_t \cdot 2NRF_{\max}^{2(N-1)}V_{\max} + \alpha_t \cdot \frac{2\lambda NRF_{\max}^{2(N-1)}V_{\max}}{\mathcal{N}_{t-1}(s_t, a_t) + \epsilon}. \end{aligned} \quad (113)$$

This is exactly the bound (A.3), completing the proof. \square

A.3 Proof of Proposition 2

We first restate Proposition 2 in precise mathematical form.

Proposition 2[Restatement] Fix a state $s \in \mathcal{S}$ and an action $a \in \mathcal{A}$. Recall the EUGE selection rule (11):

$$\text{EU}_t(s, a) = \hat{Q}_{t-1}(s, a) + c \left(\Delta Q_{t-1}(s, a) + \sqrt{\frac{\log \mathcal{N}_{\text{total}, t-1}(s)}{\mathcal{N}_{t-1}(s, a) + 1}} \right), \quad (114)$$

where $\mathcal{N}_{\text{total},t-1}(s) = \sum_{a'} \mathcal{N}_{t-1}(s, a')$ is the total visits to state s , and $c > 0$ is the exploration parameter. Suppose there exist $\delta > 0$ and $t_0 \geq 1$ such that for all $t \geq t_0$:

$$(i) \quad \hat{Q}_{t-1}(s, a) \leq \max_{a'} \hat{Q}_{t-1}(s, a') - \delta \quad (\text{suboptimality margin});$$

$$(ii) \quad c \cdot \Delta \mathcal{Q}_{t-1}(s, a) \leq \delta/4 \quad (\text{small decomposition-error bonus}).$$

Then the total number of times a is selected at s up to horizon T satisfies

$$\sum_{t=1}^T \mathbf{1}\{s_t = s, a_t = a\} \leq t_0 + \frac{16c^2}{\delta^2} \log T. \quad (\text{A.4})$$

The bound (A.4) shows that actions satisfying conditions (i)-(ii) are selected only $O(\log T)$ times. This formalizes the claim that EUGE avoids wasteful re-selection of suboptimal low-uncertainty actions.

Proof. The proof uses a counting argument based on the EUGE index structure defined in (11). The key insight is that the UCB-type exploration bonus decays as an action accumulates visits, which limits how often such an action can be chosen.

Step 1: EUGE Selection Rule.

By the EUGE rule in Algorithm 2, the action selected at time t in state s_t is:

$$a_t = \arg \max_{a' \in \mathcal{A}} \text{EU}_t(s_t, a'), \quad (115)$$

where the EUGE score is defined as:

$$\text{EU}_t(s_t, a') = \hat{Q}_{t-1}(s_t, a') + c \left(\Delta \mathcal{Q}_{t-1}(s_t, a') + \sqrt{\frac{\log \mathcal{N}_{\text{total},t-1}(s_t)}{\mathcal{N}_{t-1}(s_t, a') + 1}} \right). \quad (116)$$

The EUGE score consists of three components:

- The estimated Q-value $\hat{Q}_{t-1}(s_t, a')$;
- The decomposition error bonus $c \cdot \Delta \mathcal{Q}_{t-1}(s_t, a')$, which captures uncertainty from recent changes in the Q-estimate;

- The UCB-type bonus $c\sqrt{\frac{\log \mathcal{N}_{\text{total},t-1}(s_t)}{\mathcal{N}_{t-1}(s_t, a') + 1}}$, which encourages exploration of less-visited actions.

Step 2: Selection Implies Large EUGE Bonus.

Suppose action a is selected at state s at time t . Let $a^* = \arg \max_{a'} \hat{Q}_{t-1}(s, a')$ denote the greedy action (the action with the highest estimated Q-value).

Since a is selected, its EUGE score must be at least as large as that of any other action, including a^* :

$$\text{EU}_t(s, a) \geq \text{EU}_t(s, a^*). \quad (117)$$

We derive a lower bound on $\text{EU}_t(s, a^*)$. By definition:

$$\text{EU}_t(s, a^*) = \hat{Q}_{t-1}(s, a^*) + c \left(\Delta Q_{t-1}(s, a^*) + \sqrt{\frac{\log \mathcal{N}_{\text{total},t-1}(s)}{\mathcal{N}_{t-1}(s, a^*) + 1}} \right). \quad (118)$$

Since both $\Delta Q_{t-1}(s, a^*) \geq 0$ (by definition as an absolute value) and $\sqrt{\frac{\log \mathcal{N}_{\text{total},t-1}(s)}{\mathcal{N}_{t-1}(s, a^*) + 1}} \geq 0$, the EUGE bonus is non-negative:

$$c \left(\Delta Q_{t-1}(s, a^*) + \sqrt{\frac{\log \mathcal{N}_{\text{total},t-1}(s)}{\mathcal{N}_{t-1}(s, a^*) + 1}} \right) \geq 0. \quad (119)$$

Therefore:

$$\text{EU}_t(s, a^*) \geq \hat{Q}_{t-1}(s, a^*). \quad (120)$$

Combining (117) and (120):

$$\text{EU}_t(s, a) \geq \hat{Q}_{t-1}(s, a^*). \quad (121)$$

Expanding $\text{EU}_t(s, a)$:

$$\hat{Q}_{t-1}(s, a) + c \left(\Delta Q_{t-1}(s, a) + \sqrt{\frac{\log \mathcal{N}_{\text{total},t-1}(s)}{\mathcal{N}_{t-1}(s, a) + 1}} \right) \geq \hat{Q}_{t-1}(s, a^*). \quad (122)$$

Rearranging to isolate the EUGE bonus:

$$c \left(\Delta Q_{t-1}(s, a) + \sqrt{\frac{\log \mathcal{N}_{\text{total}, t-1}(s)}{\mathcal{N}_{t-1}(s, a) + 1}} \right) \geq \hat{Q}_{t-1}(s, a^*) - \hat{Q}_{t-1}(s, a). \quad (123)$$

Step 3: Applying Conditions (i) and (ii).

Now suppose $t \geq t_0$ and both conditions (i) and (ii) hold.

By condition (i), the value gap satisfies:

$$\hat{Q}_{t-1}(s, a) \leq \max_{a'} \hat{Q}_{t-1}(s, a') - \delta = \hat{Q}_{t-1}(s, a^*) - \delta. \quad (124)$$

Rearranging:

$$\hat{Q}_{t-1}(s, a^*) - \hat{Q}_{t-1}(s, a) \geq \delta. \quad (125)$$

Substituting (125) into (123): if action a is selected at time $t \geq t_0$, then:

$$c \left(\Delta Q_{t-1}(s, a) + \sqrt{\frac{\log \mathcal{N}_{\text{total}, t-1}(s)}{\mathcal{N}_{t-1}(s, a) + 1}} \right) \geq \delta. \quad (126)$$

By condition (ii), the decomposition-error bonus is bounded:

$$c \cdot \Delta Q_{t-1}(s, a) \leq \frac{\delta}{4}. \quad (127)$$

Substituting (127) into (126):

$$\begin{aligned} \delta &\leq c \left(\Delta Q_{t-1}(s, a) + \sqrt{\frac{\log \mathcal{N}_{\text{total}, t-1}(s)}{\mathcal{N}_{t-1}(s, a) + 1}} \right) \\ &= c \cdot \Delta Q_{t-1}(s, a) + c \sqrt{\frac{\log \mathcal{N}_{\text{total}, t-1}(s)}{\mathcal{N}_{t-1}(s, a) + 1}} \\ &\leq \frac{\delta}{4} + c \sqrt{\frac{\log \mathcal{N}_{\text{total}, t-1}(s)}{\mathcal{N}_{t-1}(s, a) + 1}}. \end{aligned} \quad (128)$$

Rearranging to isolate the UCB term:

$$c \sqrt{\frac{\log \mathcal{N}_{\text{total}, t-1}(s)}{\mathcal{N}_{t-1}(s, a) + 1}} \geq \delta - \frac{\delta}{4} = \frac{4\delta - \delta}{4} = \frac{3\delta}{4}. \quad (129)$$

Step 4: Converting to a Visit Count Bound.

We now convert the inequality (129) into an upper bound on the visit count $\mathcal{N}_{t-1}(s, a)$.

Squaring both sides of (129) (both sides are non-negative):

$$c^2 \cdot \frac{\log \mathcal{N}_{\text{total}, t-1}(s)}{\mathcal{N}_{t-1}(s, a) + 1} \geq \frac{9\delta^2}{16}. \quad (130)$$

Rearranging to solve for $\mathcal{N}_{t-1}(s, a) + 1$: multiply both sides by $(\mathcal{N}_{t-1}(s, a) + 1)$ and divide by $\frac{9\delta^2}{16}$:

$$\mathcal{N}_{t-1}(s, a) + 1 \leq \frac{c^2 \log \mathcal{N}_{\text{total}, t-1}(s)}{\frac{9\delta^2}{16}} = \frac{16c^2 \log \mathcal{N}_{\text{total}, t-1}(s)}{9\delta^2}. \quad (131)$$

Subtracting 1 from both sides:

$$\mathcal{N}_{t-1}(s, a) \leq \frac{16c^2 \log \mathcal{N}_{\text{total}, t-1}(s)}{9\delta^2} - 1 < \frac{16c^2 \log \mathcal{N}_{\text{total}, t-1}(s)}{9\delta^2}. \quad (132)$$

Since the total visits to state s cannot exceed the total number of time steps, we have $\mathcal{N}_{\text{total}, t-1}(s) \leq t - 1 \leq T$ for $t \leq T$. Taking logarithms (which is monotone increasing):

$$\log \mathcal{N}_{\text{total}, t-1}(s) \leq \log T. \quad (133)$$

Substituting into (132): selection at any $t \in [t_0, T]$ requires:

$$\mathcal{N}_{t-1}(s, a) < \frac{16c^2 \log T}{9\delta^2}. \quad (134)$$

Step 5: Counting Total Selections.

Let $n_T(s, a) := \sum_{t=1}^T \mathbf{1}\{s_t = s, a_t = a\}$ denote the total number of times action a is selected at state s up to time T .

We split this count into two periods: before time t_0 and from t_0 to T :

$$n_T(s, a) = n_{t_0-1}(s, a) + [n_T(s, a) - n_{t_0-1}(s, a)], \quad (135)$$

where $n_{t_0-1}(s, a) = \sum_{t=1}^{t_0-1} \mathbf{1}\{s_t = s, a_t = a\}$ is the number of selections before time t_0 .

Bound on selections before t_0 : Since at most one action can be selected per time step, and there are $t_0 - 1$ time steps before t_0 :

$$n_{t_0-1}(s, a) \leq t_0 - 1. \quad (136)$$

Bound on selections from t_0 to T : For $t \in [t_0, T]$, we use the visit count bound (134).

Each time action a is selected at state s , the visit count $\mathcal{N}_t(s, a)$ increases by 1. Selection at time t can only occur if $\mathcal{N}_{t-1}(s, a) < \frac{16c^2 \log T}{9\delta^2}$.

Starting from $\mathcal{N}_{t_0-1}(s, a) \geq 0$, consider the sequence of selections at times $t_0 \leq t_{(1)} < t_{(2)} < \dots \leq T$. After the k -th selection (at time $t_{(k)}$), we have $\mathcal{N}_{t_{(k)}}(s, a) = \mathcal{N}_{t_{(k)}-1}(s, a) + 1 \geq k$.

For the $(k+1)$ -th selection to occur at some time $t_{(k+1)} > t_{(k)}$, we need $\mathcal{N}_{t_{(k+1)}-1}(s, a) < \frac{16c^2 \log T}{9\delta^2}$. Since $\mathcal{N}_{t_{(k+1)}-1}(s, a) \geq \mathcal{N}_{t_{(k)}}(s, a) \geq k$, we need:

$$k < \frac{16c^2 \log T}{9\delta^2}. \quad (137)$$

Therefore, the maximum number of selections in $[t_0, T]$ is bounded by:

$$n_T(s, a) - n_{t_0-1}(s, a) \leq \left\lfloor \frac{16c^2 \log T}{9\delta^2} \right\rfloor + 1 \leq \frac{16c^2 \log T}{9\delta^2} + 1. \quad (138)$$

Combining the bounds: Substituting (136) and (138) into (135):

$$\begin{aligned} n_T(s, a) &\leq (t_0 - 1) + \frac{16c^2 \log T}{9\delta^2} + 1 \\ &= t_0 + \frac{16c^2 \log T}{9\delta^2}. \end{aligned} \quad (139)$$

Step 6: Simplifying the Constant.

We simplify the bound (139) by relaxing the constant $\frac{16}{9}$ to 16.

Since $\frac{16}{9} \approx 1.78 < 2 < 16$, we have:

$$\frac{16c^2 \log T}{9\delta^2} < \frac{16c^2 \log T}{\delta^2}. \quad (140)$$

Therefore:

$$n_T(s, a) \leq t_0 + \frac{16c^2}{\delta^2} \log T, \quad (141)$$

which is exactly the bound (A.4). This completes the proof. \square

B Parameter Matching Methodology

To ensure a fair comparison between tensor-based methods (TEQL, TLR), CUR-based methods (LoRa-VI), and deep reinforcement learning baselines (DQN, SAC), we carefully match the number of learnable parameters across all algorithms.

B.1 Parameter Formulas

TEQL and TLR represent the Q-function using a rank- R CP decomposition of a tensor $Q \in \mathbb{R}^{d_1 \times d_2 \times \dots \times d_n}$, where each d_i corresponds to the number of discretization buckets. The total parameter count is

$$P_{\text{CP}} = R \cdot \sum_{i=1}^n d_i. \quad (142)$$

DQN uses a multilayer perceptron with input dimension d_{in} , hidden layer width h , and output dimension d_{out} :

$$P_{\text{DQN}} = d_{\text{in}} \cdot h + h + h \cdot d_{\text{out}} + d_{\text{out}}. \quad (143)$$

SAC employs three such networks plus a temperature parameter: $P_{\text{SAC}} = 3 \times P_{\text{network}} + 1$.

LoRa-VI follows the CUR decomposition approach of [Stojanovic et al. \(2024a\)](#), which stores a skeleton of the Q-matrix with K anchor rows and columns:

$$P_{\text{CUR}} = K \cdot (|\mathcal{S}| + |\mathcal{A}| - K), \quad (144)$$

where $|\mathcal{S}| = \prod_i d_i^{\text{state}}$ is the total number of discretized states. To match our parameter budgets, CUR requires substantially coarser discretization than CP: for CartPole, only 3 buckets per state dimension (versus 10-20 for CP), and for Pendulum, 7 buckets per dimension (versus 20 for CP).

B.2 Parameter Configurations

Table 2 summarizes the matched parameter configurations across all environments and methods. For Highway, CUR-based LoRa-VI becomes infeasible. The 9-dimensional state

Table 2: Parameter configurations for all environments and methods.

Environment	Algorithm	Architecture	Params	Ratio
CartPole	TEQL/TLR	$R = 10$, dims=[10,10,20,20,10]	700	1.00×
	DQN	hidden=[46], in=4, out=10	696	0.99×
	SAC	hidden=[38]×3, in=4, out=10	703	1.00×
	LoRa-VI	$K = 9$, state=[3,3,3,3], $ \mathcal{A} =10$	738	1.05×
Pendulum	TEQL/TLR	$R = 10$, dims=[20,20,10]	500	1.00×
	DQN	hidden=[38], in=2, out=10	504	1.01×
	SAC	hidden=[31]×3, in=2, out=10	502	1.00×
	LoRa-VI	$K = 10$, state=[7,7], $ \mathcal{A} =10$	490	0.98×
Highway	TEQL/TLR	$R = 20$, dims=[20×9, 5]	3,700	1.00×
	DQN	hidden=[246], in=9, out=5	3,695	1.00×
	SAC	hidden=[82]×3, in=9, out=5	3,706	1.00×
	LoRa-VI	infeasible (see below)		

space yields $|\mathcal{S}| = \prod_i d_i$, which grows exponentially with dimensionality. Even with the coarsest discretization of 2 buckets per dimension, the state space contains $|\mathcal{S}| = 2^9 = 512$

states, resulting in $P_{\text{CUR}} = 20 \times (512 + 5 - 20) = 9,940$ parameters, far exceeding the budget of 3,700. This fundamental limitation demonstrates the advantage of CP decomposition, which exploits the factored structure of the state space to achieve parameter complexity of $O(\sum_i d_i)$ rather than $O(\prod_i d_i)$. **Remarks.** Hyperparameters such as batch size, buffer size, and learning rate do not contribute to the parameter count. Target networks in DQN and SAC are copies of the main networks and thus counted only once. By equalizing parameters across methods, observed performance differences reflect algorithmic properties rather than model capacity.